Studies on Cell Biological Modulation of Abnormally Accumulated Microtubule-Associated Protein Tau for Alzheimer's Disease Drug Discovery

Studies on Cell Biological Modulation of Abnormally Accumulated Microtubule-Associated Protein Tau for Alzheimer's Disease Drug Discovery

A Dissertation Submitted to

the Graduate School of Life and Environmental Sciences,

the University of Tsukuba

in Partial Fulfillment of the Requirements

for the Degree of Doctor of Philosophy in Biological Science

(Doctoral Program in Biological Sciences)

Yumiko IKEMOTO

Table of Contents

Abstract

Alzheimer's disease (AD) is a severe neurodegenerative disorder. There is no disease modifying drugs for AD so far, hence increase of number of AD patients due to population aging is a global social issue. Neurofibliraly tangles (NFTs) is a major pathological hallmarks of AD and mainly composed of tau protein. Since tau has pivotal role in the pathogenesis of AD and other tauopathy diseases, it is important to understand the cell biological basis of abnormal production and accumulation for the AD drug discovery. For this purpose, I studied about cell biological modulation of abnormal production and accumulation of tau.

In the first chapter, I describe the tau gene expression modulation through transcription factor Sp1. The tau protein is encoded by microtubule-associated protein tau (MAPT) gene and Sp1 binds to the promoter region of MAPT gene. As Sp1 is supposed to affect AD pathology via regulating tau/MAPT gene expression, targeting Sp1 is attractive strategy to modulating tau gene expression. To investigate basic information of Sp1 as a drug target, I prepared a series of Sp1 mutant proteins and examined DNA recognition properties of Sp1. From the analysis, I found that each of three zinc finger motifs had different role in DNA recognition. I also found that the C-terminal finger induced conformation change in DNA structure of the N-terminal finger binding regions, and that the conformation change affected DNA recognition mode of the N-terminal finger. These findings are useful for designing tau expression modulator targeting Sp1.

In the second chapter, I describe a novel glycogen synthase kinase-3 (GSK-3) inhibitor that suppresses tau phosphorylation. Tau is hyperphosphorylated mainly by glycogen synthase kinase 3 (GSK-3). Accordingly GSK-3 inhibitor is expected to improve AD pathology by inhibiting NFT formation. I discovered a potent and selective GSK-3 inhibitor, compound A and found that compound A reduced tau phosphorylation *in vitro* and *in vivo*. And chronic treatment of compound A in human P301L tau expressing mouse (JNPL3 mice, an AD mice model) resulted in significant reduction on not only tau phosphorylation but also abnormal tau aggregation.

Taken together, I conclude that cell biological modulation of tau gene expression and tau phosphorylation is attractive strategy for AD treatment, and tau–targeting approach is promising beyond 'Aβ hypothesis' based approach.

Abbreviations

Aβ	amyloid β
AD	Alzheimer’s disease
ATP	adenosine triphosphate
DNA	deoxyribonucleic acid
GSK-3	glycogen synthase kinase-3
MAPT	microtubule associated protein tau
NFT	neurofibliraly tangle
Sp1	specificity protein 1
SEM	standard error of mean

General Introduction

AD is a severe and progressive neurodegenerative disorder with cognitive impairment and personality change due to synaptic and neuronal loss. AD is a most common dementia accounting for estimated 60 to 80 percent of cases. Worldwide, nearly 44 million people have AD or related dementia, and AD is now 4th leading cause of death in the high income countries in the world (1). The global cost of AD and dementia is estimated to be $818 billion in 2015 (1). Increase of number of AD patients due to population aging is a global social issue. Currently, there is no disease modifying drugs for AD with limited treatment options of symptomatic relief.

The two major pathological hallmarks in brains of AD patients are senile plaques composed of Aβ peptides and NFTs composed of abnormally hyperphosphorylated tau protein. Aβ targeting drug development/therapies have widely been researched and developed for AD treatment, and this strategy has strongly supported by the discovery of disease associated mutations in Aβ-related genes, such as amyloid precursor protein, Presenilin-1, and Presenilin-2. Nevertheless, several large clinical trials of Aβ targeting drug candidates for the treatment of AD and mild cognitive impairment have failed over the last decade. Recent multicenter neuroimaging study results indicated that Aβ pathology (senile plaques) appeared in the very early stages of AD pathology development and preceded clinical symptom, suggesting the necessity of the very early intervention and prevention for Aβ targeting treatment (2).

Recent growing number of evidences supports the idea that NFT is a key driver of disease progression in AD (3), and people pay much attention to tau targeting strategy for AD drug development. Tau is a microtubule associated protein and mostly localized in axons. Physiologically, tau has an important role in microtubule assembly and microtubule stability, also contributes maintaining normal axonal integrity and neuronal function (4-6). Tau is supposed to have other functions, such as cellular signaling, neuronal development, neuroprotection, and apoptosis (4-6). In spite of its important roles in cellular processes, several lines of tau knockout

mice were reported to be viable and do not display any gross physical or behavioral abnormalities, as microtubule associated protein 1A (MAP1A) may compensate for the loss of tau (4). In AD and other tauopathy patient brains, such as Pick's disease (PiD) frontotemporal dementia with Parkinsonism linked to chromosome 17 (FTDP-17), progressive supranuclear palsy (PSP), and corticobasal degeneration (CBD), abnormally hyperphosphorylated tau accumulate as paired helical filaments (PHF) (5). Abnormally hyperphosphorylated tau is dissociated from microtubule, leading to neuronal damage with impaired axonal transport (5). Disease associated mutation in MAPT gene were reported in frontotemporal lobar degeneration with parkinsonism 17 (FTDP-17) patients (7).

Since tau has pivotal role in the pathogenesis of AD and other tauopathy diseases, it is necessary to understand the basis of abnormal production and accumulation for the AD drug discovery. For this purpose, I studied about cell biological modulation of abnormal production and accumulation of tau. In the first chapter, I describe the tau gene expression modulation through transcription factor Sp1. Tau is encoded by MAPT gene and Sp1 binds to the promoter region of MAPT gene (8). In AD and other tauopathy patient postmortem brains, Sp1 is abnormally expressed (9). As Sp1 is supposed to affect AD pathology via regulating tau/MAPT gene expression, targeting Sp1 is attractive strategy to modulating tau gene expression. To investigate basic information of Sp1 as drug target, I prepared a series of Sp1 mutant proteins and examined DNA recognition properties of Sp1. In the second chapter, I describe a novel GSK-3 inhibitor that suppresses tau phosphorylation. I discovered a potent and selective GSK-3 inhibitor, compound A and found that compound A reduced tau phosphorylation *in vitro* and *in vivo*. And chronic treatment of compound A in human P301L tau expressing mouse (JNPL3 mice, an AD mouse model) resulted in significant reduction on not only tau phosphorylation but also abnormal tau aggregation.

Part I

Finger-positional change in three zinc finger protein Sp1

: influence of terminal finger in DNA recognition.

Abstract

The connection of functional modules is effective for the design of DNA binding molecules with the desired sequence specificity. C2H2-type zinc finger proteins have a tandemly repeated array structure consisting of independent finger modules and are expected to recognize any DNA sequences by permutation, multi-connection, and the substitution of various sets of zinc fingers. To investigate the effects of the replacement of the terminal finger on the DNA recognition by other fingers, I have constructed the three zinc finger peptides with finger substitution at the N- or C-terminus, Sp1(zf223), Sp1(zf323), and Sp1(zf321). From the results of gel mobility shift assays, each mutant peptide binds preferentially to the target sequence that is predicted if the fingers act in a modular fashion. The methylation interference analyses demonstrate that in the cases of the N-terminal finger substitution mutants, Sp1(zf223) and Sp1(zf323), the N-terminal finger recognizes bases to different extents from that of the wild-type peptide, Sp1(zf123). Of special interest is the fact that the N-terminal finger of the C-terminal finger substitution mutant, Sp1(zf321), shows a distinct base recognition from those of Sp1(zf123) and Sp1(zf323). DNase I footprinting analyses indicate that the C-terminal finger (active finger) induces a conformational change in the DNA in the region for the binding of the N-terminal finger (passive finger). The present results strongly suggest that the extent of base recognition of the N-terminal finger is dominated by the binding of the C-terminal finger. This information provides an important clue for the creation of a zinc finger peptide with the desired specificity, which is applicable to the design of novel drugs and biological tools.

Introduction

The design of DNA targeting proteins with desired functions is one of the most significant problems in the post-genome era and may lead to the creation of new drugs and biological tools. To achieve this goal, it is necessary to establish the DNA recognition rule by the DNA binding molecules with a well-defined modular structure such as the C2H2-type zinc finger and pyrrole−imidazole polyamide (10, 11). The C2H2-type zinc finger motif has a tandemly repeated structure consisting of independent modules with the consensus sequence: (Tyr,Phe)-X-Cys-X2,4-Cys-X3-Phe-X5-Leu-X2-His-X3-5-His-X2-6. Each finger domain is mostly connected by a well-conserved linker and has a compact globular ββα structure due to tetrahedral binding of a zinc ion with invariant cysteines and histidines. The first crystal structural analysis of the Zif268−DNA complex has provided useful information about the DNA recognition by the C2H2-type zinc finger motif (12, 13). In the complex, each zinc finger makes direct base contacts by using amino acids at positions −1, 2, 3, and 6 in the α-helix that recognizes overlapping four-base-pair subsites mainly on the guanine-rich strands of the binding site. However, two unique features opposed to the modularity of the zinc finger have been reported in the DNA recognition by the zinc finger protein. One is the unbalanced influence of these fingers on the DNA binding observed in the DNA bindings of Zif268 (14), the C-terminal three fingers of TFIIIA (15), and WT1 (16). In them, the N-terminal fingers make particularly smaller contributions to the high-affinity DNA binding than the other fingers. The other influence is the relative finger position on the DNA binding of the finger. The order change of zinc fingers in an array and sequential selection via the phage display give rise to the unexpected effects on the DNA base recognition by zinc fingers (17, 18).

Transcription factor Sp1 is a sequence-specific DNA binding protein derived from the HeLa cell (19, 20). Sp1 has three contiguous repeats of a C2H2-type zinc finger motif at the C-terminus and activates transcription in various viral and cellular genes by binding to the GC box, which has the decanucleotide consensus sequence 5'-(G/T)GGGCGG(G/A)(G/A)(C/T)-3' (20−24). Together with the crystallographic evidence of the Zif268−DNA complex, some previous studies about the Sp1−DNA interaction revealed that the three zinc fingers of Sp1 also make a different contribution to GC-box DNA binding (25-28). Namely, the contribution is reduced in the order: C-terminal finger > central finger > N-terminal finger. Moreover, the N-terminal zinc finger of Sp1 uniquely binds to DNA, whereas the central and C-terminal zinc fingers typically bind to DNA (28). The finger does not utilize His(3), but instead utilizes Lys(−1) for the recognition of the guanine bases at the center and the 3'-end of the 5'-GGG-3' subsite despite prevalent recognition of guanine at the center of the 5'-GGG-3' subsite by His(3).

In this study, I prepared three mutant zinc finger peptides, Sp1(zf223), Sp1(zf323), and Sp1(zf321), and evaluated the effect of the terminal finger on the base recognition of the other fingers in the DNA binding of three zinc finger peptide. The wild-type and mutant peptides preferably bind to their predicted binding sequences. Methylation interference and DNase I footprinting analyses suggest that the different degrees of base recognition of the N-terminal finger of the mutant peptides from that of wild type is due to the DNA conformational change induced by the binding of the C-terminal finger.

Materials and Methods

Materials

All enzymes were purchased from New England Biolabs (Beverly, MA, USA), except for the restriction enzyme *Age*I obtained from Nippon Gene (Tokyo, Japan). The synthesized oligonucleotides for construction of the genes and substrate DNAs were acquired from Amersham Pharmacia Biotech (Piscataway, NJ, USA). Labeled compound [γ-32P]ATP was supplied by DuPont (Wilmington, DE, USA). The plasmid pBS-Sp1-fl was kindly provided by Dr. R. Tjian. All other chemicals were of commercial reagent grade.

Preparation of Zinc Finger Peptides from Sp1

The primary structures of all the zinc finger peptides used in this study are summarized in Figure 1A. Sp1(zf123), which is the alias for Sp1(530−623), is coded on plasmid pEVSp1(530−623) as previously described (29). For the creation of Sp1(zf223) and Sp1(zf323), the finger 2, 3, and 2−3 gene fragments were amplified by PCR with the primer set of pEVSp1(530−623) as a template. The amplified single-finger fragments were designed to be flanked by the N-terminal region with the *Bam*HI site at the 5'-end and the *Age*I site at the 3'-end. On the other hand, the double-finger fragments were amplified aite at the 5'- and 3'-ends, respectively. The *Age*I enzyme site in the linker region encodes amino acids Thr-Gly, part of the linker peptide between fingers 1 and 2. By digesting one set of single- and double-finger fragments with enzymes and ligating them into the similarly digested pEV3b, I constructed the plasmids pEVSp1(zf223) and pEVSp1(zf323), which code Sp1(zf223) and Sp1(zf323), respectively. The plasmid pEVSp1(zf321) coding Sp1(zf321) was created by ligating the N-terminal double-finger gene fragment from pEVSp1(zf323) and the finger 1 gene fragment from

pEVSp1(530−623) in the same manner as described above. All sequences were confirmed by the BcaBEST Dideoxy Sequencing Kit (Takara Shuzo, Kyoto, Japan). These zinc finger peptides were overexpressed in *Escherichia coli* strain BL21(DE3)pLysS and purified as previously described (28), except for the use of 1 mM dithiothreitol as the reductant.

Preparation of Substrate DNA Fragments

The substrate oligonucleotides contain the target binding site predicted from the binding mode of the transcription factor Sp1: GC(123), 5'-GGG GCG GGGCC-3'; GC(223), 5'-GGG GCG GCGGC-3'; GC(323), 5'-GGG GCG GGGGC-3'; GC(321)-1, 5'-GGGC GCG GGGGC-3'; and GC(321)-2, 5'-GGGCC GCG GGGGC-3'. The synthesized oligonucleotides were annealed and inserted in pBluescript II SK+ (Stratagene, La Jolla, CA, USA). The *Hind*III−*Xba*I fragment was cut out and labeled at the 5’-end by ^{32}P for the experiments.

Circular Dichroism (CD) Measurements

The CD spectra of the wild-type and mutant zinc finger peptides of Sp1 were recorded on a Jasco J-720 spectropolarimeter in 10 mM Tris-HCl (pH 8.0), 50 mM NaCl, 1 mM dithiothreitol, and 5 μM zinc finger peptide at 20°C.

Gel Mobility Shift Assays

Gel mobility shift assays were carried out under the following conditions. Each reaction mixture contained 10 mM Tris-HCl (pH 8.0), 50 mM NaCl, 1 mM dithiothreitol, 10 μM $ZnCl_2$, 25 ng/μL poly(dI-dC), 0.05% Nonidet P-40, 5% glycerol, 40 mg/μL BSA, the ^{32}P-end-labeled substrate DNA fragment (~50 pM), and 0−4 μM zinc finger peptide. After incubation at 20°C for 30 min, the sample was run on a 12% polyacrylamide gel with Tris−borate buffer at 20°C. The

bands were visualized by autoradiography and quantified with NIH image software (version 1.62). The dissociation constants (Kd) of the Sp1 peptide−DNA fragment complexes were estimated based on a previously reported procedure (28).

Methylation Interference Analyses

Methylation interference assays were investigated as previously described (27, 29). The binding reaction mixture contained 10 mM Tris-HCl (pH 8.0), 50 mM NaCl, 1 mM dithiothreitol, 10 μM $ZnCl_2$, 20 or 25 ng/μL competitor DNA, 0.05% Nonidet P-40, 5% glycerol, the ^{32}P-end-labeled methylated DNA fragment (~40 nM, 400 Kcpm), and 10−500 nM zinc finger peptides. As competitor DNAs, 20 ng/μL sonicated calf thymus DNA and 25 ng/μL poly(dI-dC) were used for the experiments shown in Figures 3 and 4, respectively. To examine both the strong and weak base contacts in the methylation interference experiment, I selected the experimental conditions such that the peptide/DNA molar ratio in the binding reaction was about 10−20% bound. Densitometric measurements were obtained with NIH image software (version 1.62). The extent of interference was estimated as previously described (28).

DNase I Footprinting Analyses

DNase I footprinting experiments were performed according to the method of Brenowitz *et al.* (30). The binding reaction mixture contained 20 mM Tris-HCl (pH 8.0), 15 mM NaCl, 5 mM $CaCl_2$, 10 mM $MgCl_2$, 20 ng/μL sonicated calf thymus DNA, the 5‘-end-labeled substrate DNA fragment (~8 nM, 20 000 cpm), and 0−10 μM peptide. After incubation at 20°C for 30 min, the sample was digested with DNase I (0.75 milliunit/μL) at 20°C for 2 min. The reaction was stopped by the addition of 20 μL of DNase I stop solution (0.1 M EDTA and 0.6 M sodium acetate) and 100 μL of ethanol. After ethanol precipitation, the cleavage products were analyzed

on a 10% polyacrylamide/7 M urea sequencing gel. The bands were visualized by autoradiography.

Results

Design of Mutant Zinc Finger Peptides, Sp1(zf223), Sp1(zf323), and Sp1(zf321) and Their Predicted Binding Sequences

To study the effect of the terminal finger of the three finger peptide on DNA binding of the peptide, I prepared three mutant zinc finger peptides, Sp1(zf223), Sp1(zf323), and Sp1(zf321) (Figure 1A, left panel). Sp1(zf223) and Sp1(zf323), in which the N-terminal finger 1 of Sp1(zf123) is replaced with fingers 2 and 3, respectively, are the mutants for the evaluation of the N-terminal finger properties. On the other hand, the effect of replacing the C-terminal finger on the DNA binding mode is estimated by the preparation of a mutant peptide, Sp1(zf321), which has three zinc fingers arrayed inversely in comparison with Sp1(zf123). Previous study demonstrated that the finger 3-deleted mutant, Sp1(zf12), formed no stable complex with the GC-box DNA under my experimental conditions because of the small contribution of finger 1 to the DNA binding (28). Therefore, I did not design Sp1(zf121) but Sp1(zf321), considering the deficiency of the DNA binding ability of Sp1(zf121).

The predicted binding sequences, which are designed from the putative DNA binding mode of Sp1 (Figure 1B; 28), are shown in Figure 1A (right panel). The wild-type GC-box sequence, GC(123), is derived from the mouse dihydrofolate reductase promoter (I and III) (18, 19). GC(223) and GC(323) are the target sequences for Sp1(zf223) and Sp1(zf323), respectively. From the results of the previous interference experiment for Sp1(zf123), finger 1A of Sp1(zf123) recognizes uniquely the five-base-pair subsite (28). On the contrary, the zinc finger proteins such as Zif268 exhibit the typical recognition of the three-base-pair subsite by each finger domain (12). To clarify whether the base recognition mode of finger 1C of Sp1(zf321) is typical or unique, I

prepared two sequences, GC(321)-1 and -2, in addition to GC(321)-0 which is identical to the target sequence for Sp1(zf323).

Examination of the Folding Property of Wild-Type and Mutant Zinc Finger Peptides of Sp1

To examine the change in the folding property by finger substitution, I analyzed the secondary structures of the peptides based on measurements of the CD spectra. Figure 2 shows the CD measurement results for the peptides at 20°C. The spectrum for Sp1(zf123) was similar to those of the single- and three-finger peptides of Sp1 previously described (31-33). Negative Cotton effects in the far-UV region with a minimum at 206 nm and a shoulder around 222 nm suggest that Sp1 (zf123) has an ordered secondary structure. The spectrum for Sp1(zf321) was quite similar to that of Sp1(zf123). On the other hand, Sp1(zf223) and Sp1(zf323) exhibited spectra somewhat different from those of Sp1(zf123) and Sp1(zf321). As for the ellipticities at 206 nm, the values of Sp1(zf123) and Sp1(zf321) ($[\theta]_{206} = -11\,936, -10\,984$, respectively) were distinct from those of Sp1(zf223) and Sp1(zf323) ($[\theta]_{206} = -14\,205, -14\,673$, respectively). This is probably due to the difference in the composition of the fingers. These results indicate that the conformation of the finger domain in each peptide is not identical but comparable with that of each other. I obtained the same results at 4°C (data not shown).

Evaluation of the Binding Affinity of Mutant Zinc Finger Peptides to Wild-Type and Mutant GC Boxes

By using gel mobility shift assays, I obtained the dissociation constants (K_d) of these peptide−DNA complexes as summarized in Table 1. Sp1(zf123) binds to GC(123) with a 5.3 nM dissociation constant, which is comparable to the previously reported value, whereas GC(223) and GC(323) dissociation constants were 57 and 22 nM, respectively. The K_d values for the

Sp1(zf223)−GC(123), −GC(223), and −GC(323) complexes were 41, 3.9, and 21 nM, respectively. On the other hand, the Kd values for Sp1(zf323) binding to GC(123), GC(223), and GC(323) were 24, 60, and 6.6 nM, respectively. These results suggest that each mutant mentioned above binds to the predicted binding sequence with the highest affinity under my experimental condition.

On the contrary, Sp1(zf321) binds to the wild-type and mutant GC boxes with a 70−250-fold lower affinity than the other peptides. The dissociation constants of Sp1(zf321) for GC(123), GC(223), and GC(323) are 994, 286, and 314 nM, respectively, indicating that GC(223) and GC(323) are preferable to GC(123) for the binding of Sp1(zf321) to DNA. All peptides used in this study showed no effective binding to GC(321)-2. GC(321)-1 was bound only by Sp1(zf123) and Sp1(zf323) with 714 and 512 nM dissociation constants, respectively.

Specific Base Recognition Mode of Mutant Zinc Finger Peptides Revealed by Methylation Interference Analysis

Figure 3A shows the methylation interference patterns of Sp1(zf123), Sp1(zf223), and Sp1(zf323) for GC(123), GC(223), and GC(323), respectively. The extent of the interference based on a densitometric analysis is shown by histograms (Figure 3B). The interference patterns at subsites I and II were the same among these peptides. In contrast, distinct interference patterns were observed at subsite III. Namely, the recognition of G7 in Sp1(zf223) and Sp1(zf323) was 5-fold stronger than in Sp1(zf123), and the recognitions of G10 in Sp1(zf223) and Sp1(zf323) and G11' in Sp1(zf223) were almost lost. In Figure 3C, I compared the extent of the interference of fingers 2 and 3 on the basis of the difference in the relative position, suggesting that the difference has a significant effect on the base recognition of the cognate fingers.

Figure 4 shows the results of the methylation interference assay for Sp1(zf321). From the results of the evaluation of Kd, Sp1(zf321) binds to GC(223) and GC(323) with a higher affinity than the other DNAs. Therefore, I carried out an experiment using such peptide−DNA combinations in which Sp1(zf323) was employed as the control. Panels A and B depict the electrophoretic results and the densitometric analysis for Sp1(zf321), respectively. There is no obvious difference in the extent of interference between the Sp1(zf321)− and Sp1(zf323)−GC(223) complexes. In the binding to GC(323), Sp1(zf321) shows an interference pattern distinct from that of Sp1(zf323). The bases at subsite III were not strongly recognized by Sp1(zf321), as is distinct from the case with Sp1(zf323).

Analysis of Conformational Changes of DNA Induced by Binding of Mutant Zinc Finger Peptides

Figure 5 shows the DNase I footprinting patterns of Sp1(zf123), Sp1(zf223), Sp1(zf323), and Sp1(zf321) for their high-affinity binding sequences. All mutant peptides protected the wild-type or mutant GC box from cleavage by DNase I in both strands. Hypersensitive cleavage was observed at the 5'-AA-3' step outside the GC box in the guanine-rich strand (G-strand), whereas no cleavage induction by protein binding was detected in the cytosine-rich strand (C-strand). In addition, hypersensitive cleavage was also induced in the G-strand by the binding of Sp1(zf321) between G8 and G9 in the GC box. The same footprinting patterns were also obtained in the case of the wild-type and mutant Sp1 peptide−GC(123) complexes (data not shown).

Discussion

Effects of Replacement of Finger 1 in Sp1(zf123) on DNA Binding Affinity and Specificity

Based on previous mutational analyses of Sp1(zf123) and the GC boxes (28), the relative contribution of the three fingers of Sp1(zf123) to the DNA binding affinity was shown to be reduced in the order of finger 3 > finger 2 > finger 1. It is expected that the replacement of finger 1 with finger 2 or 3 in Sp1(zf123) leads to an increase in the DNA binding affinity of Sp1(zf123). The results presented here show that both Sp1(zf223) and Sp1(zf323) preferentially bind to their predicted binding sequences with a dissociation constant comparable to that of Sp1(zf123). In contrast, the deletion of finger 1 from Sp1(zf123) results in an 89-fold reduction in the binding affinity to GC(123) (28). Together with this evidence, the results indicate that these mutants evidently make use of all three fingers in DNA binding and that the N-terminal fingers, fingers 2A and 3A of Sp1(zf223) and Sp1(zf323), respectively, make an equivalent contribution to the DNA binding of finger 1A of Sp1(zf123).

The extent of base recognition of Sp1(zf223) and Sp1(zf323) appears to be distinct in part from that of Sp1(zf123). From the results of the methylation interference analyses, the two fingers at positions B and C of the mutant peptides maintain the same base recognition mode as that of Sp1(zf123). With respect to their fingers at position A, the strong interference patterns of Sp1(zf223) and Sp1(zf323) at G7 in the G-strand suggest that they recognize bases at subsite I like fingers 1 and 2 of Zif268, respectively, in contrast to finger 1A of Sp1(zf123), which recognizes G8 and G9 by Lys(−1) and exhibits a weak interference pattern at G7. The direct comparison of the extent of base recognition by them with that in their native positions demonstrates the difference in the extent of recognition (Figure 3C). In Sp1(zf323), G7 is recognized 1.5-fold stronger than G1. The extent of the recognition is also stronger than that of

G7 in Sp1(zf123) by a factor of 3.7. In the DNA binding of the zinc finger protein, the helicity of the recognition helix increases by the C-cap formation in the linkers connecting adjacent fingers at the C-terminal side (34). The increase in the recognition of G7 in the Sp1(zf323)−GC(323) complex may be elucidated by the increment of helicity induced by new C-cap formation in finger 3A of Sp1(zf323). However, the mutation of Ala(6) to arginine in finger 1A of Sp1(zf123), which was carried out for the increase in the recognition of G7 in the Sp1(zf123)−GC(123) complex considering the typical base recognition mode of the zinc finger peptide, had no drastic effect on the recognition of G7 in GC(123) despite the plausibility of the original C-cap formation in finger 1A of Sp1(zf123) (35). This evidence suggests that the extent of recognition of G7 by the finger at position A of these Sp1 peptides is undetermined only by the C-cap formation in the finger.

In contrast, the recognition of G9 by finger 2A of Sp1(zf223) is 5-fold weaker than the recognition of G6 by finger 2B. A rationale for the disruption of the base recognition by a terminal zinc finger is reported as an end effect (14). In this theory, the base recognition by the amino acids such as Arg(18) and Arg(80), which are situated at positions −1 and 6 in the α-helices of fingers 1 and 3 of Zif268, respectively, is less sensitive to the mutation to glycine than the other critical amino acid residues. This is not applicable to my system for the following reason: no decrease in the base recognition by finger 3A of Sp1(zf323) was observed, whereas a similar decrease was detected in the Sp1(zf223)−GC(223) complex.

Effects of Replacement of Finger 3 in Sp1(zf123) on DNA Binding Affinity and Specificity

Previous report revealed that finger 1A of Sp1(zf123) recognizes the five-base-pair subsite (28). On the basis of several X-ray crystallographic analyses (12, 13, 36-39), fingers 1C, 2B, and 3A of Sp1(zf321) are expected to bind to subsites I, II, and III, respectively, and the predicted binding sequence for finger 1C is not the five- but the three-base-pair site, 5‘-NGG-3‘,

in the G-strand. The actual DNA binding affinity of Sp1(zf321) for various GC boxes estimated by the calculation of the Kd values suggests that a pertinent interaction between finger 1C and subsite III does not occur in GC(321)-1 or -2, but in GC(123), GC(223), and GC(323). The inability of Sp1(zf321) binding to GC(321)-1 and -2 also demonstrates that Sp1(zf321) did not bind to the DNA by the N-terminal two-finger domain in contrast to the ability of the two-finger peptide, Sp1(zf23), to bind to GC(123) (28). This evidence indicates that the constitution and order of the finger is important for DNA binding of the zinc finger protein with a high affinity and specificity despite the sufficiency of the two-finger domain for DNA binding. For the DNA binding of the two-finger peptide composed of fingers 2 and 3, fingers 2 and 3 need to be aligned in the direction from amino- to carboxyl-termini.

As evidenced by the comparison of the results of the methylation interference analyses and estimation of the Kd values of Sp1(zf321) with those of other mutants, the base recognition mode of finger 1C of Sp1(zf321) is distinct from that of finger 1A of Sp1(zf123). Finger 1C of Sp1(zf321) appears to have the typical base recognition mode of the zinc finger protein. That is to say, Lys(−1) and His(3) recognize G3 and G2 in subsite I. G1 might be recognized by Arg(5). The base recognition by Arg(5) was also discovered in the GLI−DNA complex, in which Arg(5) in finger 5 recognizes guanine at position 4' (36). In addition, it is of special interest that the base recognition mode of finger 3A of Sp1(zf321) is clearly different from that of finger 3A of Sp1(zf323). Replacement of finger 3C by finger 1 in Sp1(zf323) induced a 15-fold reduction in the extent of recognition of G8 by finger 3A. As mentioned earlier, the extent of base recognition by the finger at position A is distinct from that of the finger at the native position in the cases of Sp1(zf223) and Sp1(zf323). Therefore, the zinc fingers at positions A and C are passive and active fingers, respectively.

Effects of Conformational Change of DNA Induced by the Binding of Active Finger on DNA Binding of Passive Finger

Several conformational changes of DNA induced by the binding of the zinc finger protein, such as bending (29, 37, 39, 40), local distortion (28), and unwinding (41), have been reported. DNA bending is induced by the bindings of Tramtrack, Sp1, and TFIIIA. Based on my CD data for the wild-type and mutant peptides, no drastic conformational change in each finger domain appears to occur, suggesting that the conformational change of DNA has effects on the DNA binding of the peptides. For the investigation of the existence of DNA bending, DNase I footprinting analyses are available, since hypersensitive cleavage of DNA by DNase I induced by the binding of protein is generally attributed to a conformational change in the DNA, in particular bending (42). In fact, such a hypersensitive cleavage has also been observed in the 3‘-region outside the GC-box in the G-strand for the binding of the zinc finger of Sp1 to the GC-box DNA, and this is consistent with the evidence of DNA bending by circular permutation analyses (28, 29, 40). Therefore, I applied DNase I footprinting analyses to the examination of the DNA bending by the Sp1 mutants. My footprinting results clearly show that Sp1(zf321) produces bending of the GC-box DNA at subsite III. The hypersensitive cleavage at the G8−G9 step does not occur in the binding of Sp1(zf323), indicating that finger substitution at position C in Sp1(zf323) induces a structural change. The other conformational change of DNA by Sp1 binding is local distortion of the GC-box DNA in the 3'-region of the G-strand revealed by previous footprinting analyses (27). In the binding of Sp1(zf123) to GC(123), finger 1A recognizes the bases of the region in a unique manner. Together with the result that finger 1 shows the typical base recognition mode by transferring from positions A to C, it is suggested that the conformational distortion has an effect on the base recognition mode and/or extent of the zinc finger at position A. Moreover, the distortion is induced by the binding of the C-terminal two fingers of Sp1(zf123) (Sogo *et al.*,

unpublished data), indicating that Sp1(zf223) and Sp1(zf323) also cause a distortion in subsite III by the C-terminal two fingers upon binding to DNA and fingers 2A and 3A may show different extents of base recognition than that in the native positions. In the mechanism described above, the N- and C-terminal fingers in the three-finger-peptide are passive and active fingers for base recognition of DNA, respectively.

In this paper, I report “the active and passive fingers mechanism in DNA recognition by three-zinc-finger peptide” which is based on the conformational change in DNA induced by the C-terminal finger. This concept is not always applicable to the DNA binding of other zinc finger proteins. In fact, all zinc fingers equivalently bind to DNA without any induction of a conformational change in DNA during the DNA binding of Zif268 and YY1 (12, 13, 38). In the N-terminal six zinc fingers of the TFIIIA−DNA complex, however, DNA is bent in the binding regions of fingers 1 and 2 (39). Recently, it was reported that the three-zinc-finger domain binds to DNA as one unit during the DNA binding of the zinc finger protein by multiconnection of identical zinc fingers (43). Therefore, in the design of zinc finger proteins with a novel sequence preference, selection of the third finger (passive finger) at the N-terminus of a two-finger domain containing an active finger is desirable. Thus far, the DNA recognition code of the zinc finger has been analyzed by a phage display method (44-47). While most of sequences can be recognized by zinc finger proteins, unrecognized sequences remain. I may overcome this problem by considering the presented information in the design of novel zinc finger peptides. Additionally, such peptides give promise of the application of the zinc finger peptide to the design of novel drugs and biological tools.

Tables and Figures

Table 1: Dissociation Constants (Kd) for Spl(zf123), Sp1(223), Sp1(zf323), and Sp1(zf321) Binding to Wild-Type (GC) and Mutant GC Boxes. a, Apparent dissociation constants were determined by titration using a gel mobility shift assay as described under Materials and Methods. Values are averages of three or more independent determinations with standard deviations. B, The nomenclature is described in the text (see Figure 1). c, ND, not determined.

	Kd (nM)[a]			
binding site[b]	Sp1(zf123)	Sp1(zf223)	Sp1(zf323)	Sp1(zf321)
GC(123)	5.3 ± 0.4	41 ± 2.2	24 ± 1.1	994 ± 45
GC(223)	57 ± 2.6	3.9 ± 0.2	60 ± 2.3	286 ± 29
GC(323)	22 ± 1.6	21 ± 1.0	6.6 ± 0.2	314 ± 15
GC(321)-1	714 ± 74	>4000	512 ± 57	>4000
GC(321)-2	>4000	>4000	>4000	ND[c]

Figure 1. (A) Primary structures of wild-type and mutant zinc finger peptides of Sp1 (left) and their predicted binding sequences (right). The designation of each zinc finger is shown by the original name (fingers 1−3) with an alphabetical letter indicating the absolute position (positions A−C). Substituted or inserted nucleotides in the mutated GC-box sequences are depicted in boldface type. The base numbers in the wild-type and mutant GC boxes are also shown. (B) Mode of putative interaction of Sp1 with GC-box DNA. Amino acid residues at the N-terminus of the α-helix in each finger are depicted by their one-letter codes with the number of helical positions below. Solid arrows show the amino acid−base contacts assumed by the DNA binding mode of Zif268, and dotted arrows depict the contacts indicated by previous report.

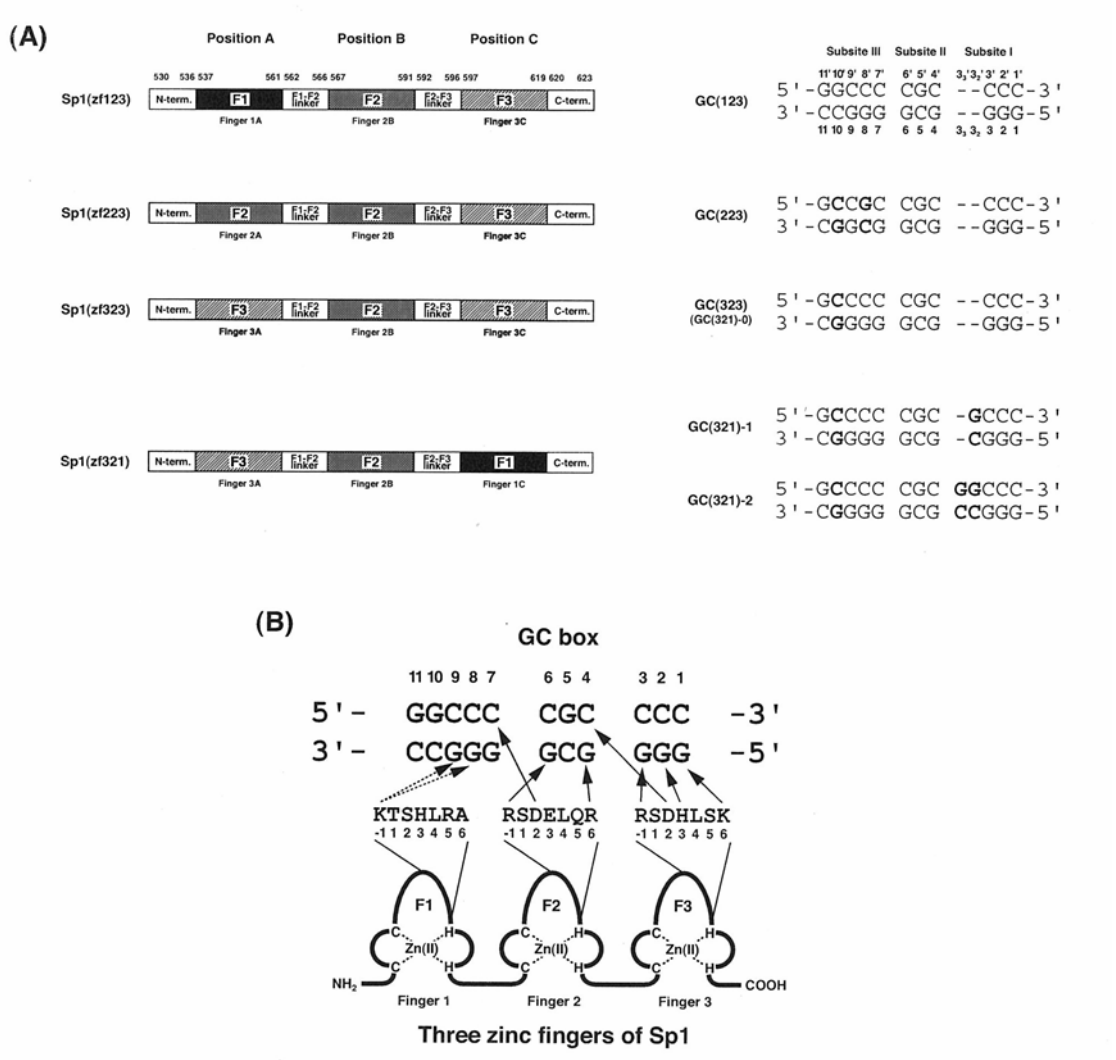
(A)
Position A
Position B
Position C
Sp1(zf123)
Sp1(zf223)
Sp1(zf323)
Sp1(zf321)
N-term.
F1
F2
F3
C-term.
Finger 1A
Finger 2A
Finger 3A
Finger 1C
Finger 2B
Finger 3C
GC(123)
GC(223)
GC(323)
(GC(321)-0)
GC(321)-1
GC(321)-2
Subsite III
Subsite II
Subsite I
(B)
GC box
5'- GGCCC CGC CCC -3'
3'- CCGGG GCG GGG -5'
KTSHLRA
RSDELQR
RSDHLSK
Zn(II)
NH2
COOH
Finger 1
Finger 2
Finger 3
Three zinc fingers of Sp1

Figure 2. CD spectra of wild-type and mutant zinc finger peptides of Sp1 at 20°C.

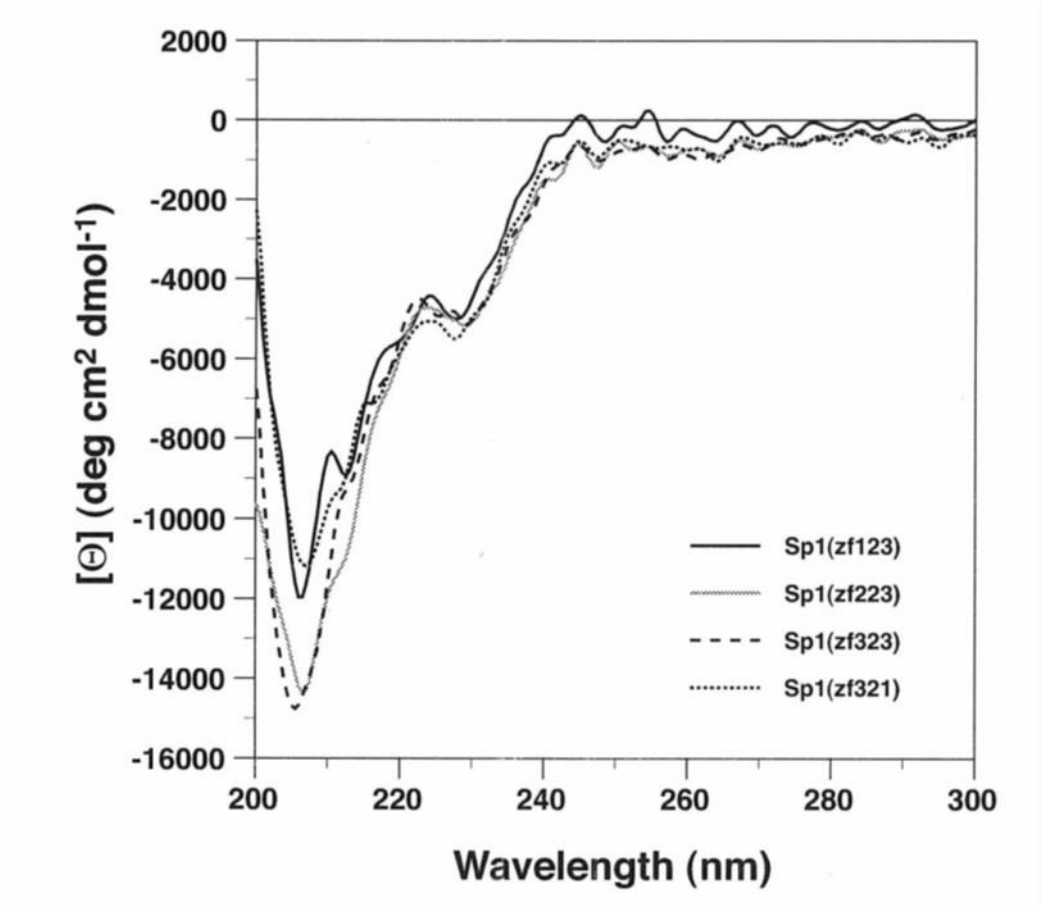
2000
0
-2000
-4000
-6000
-8000
-10000
-12000
-14000
-16000
200
220
240
260
280
300
[Θ] (deg cm2 dmol-1)
Wavelength (nm)
Sp1(zf123)
Sp1(zf223)
Sp1(zf323)
Sp1(zf321)

Figure 3. (A) Methylation interference analyses for Sp1(zf123), Sp1(zf223), and Sp1(zf323) binding to GC(123), GC(223), and GC(323), respectively. The left (lanes 1−9) and right (lanes 10−18) panels show the results for the G- and C-strands, respectively. Lanes 1, 4, and 7 and lanes 10, 13, and 16 contain G+A and C+T of the Maxam−Gilbert sequencing reactions, respectively. The remaining lanes represent free (F) and peptide-bound (B) DNA samples. In these experiments, calf thymus DNA was used as a competitor (see Materials and Methods for details). (B) A histogram showing the extent of methylation interference by Sp1(zf123), Sp1(zf223), and Sp1(zf323). Three or more autoradiograms of the gels were scanned with a densitometer, and the average extent of interference was calculated as the ratio of the cutting probabilities for the two bands (B/F). (C) Direct comparisons of the extent of interference between finger 2B of Sp1(zf123) and finger 2A of Sp1(zf223) (left) and between finger 3C of Sp1(zf123) and finger 3A of Sp1(zf323) (right).

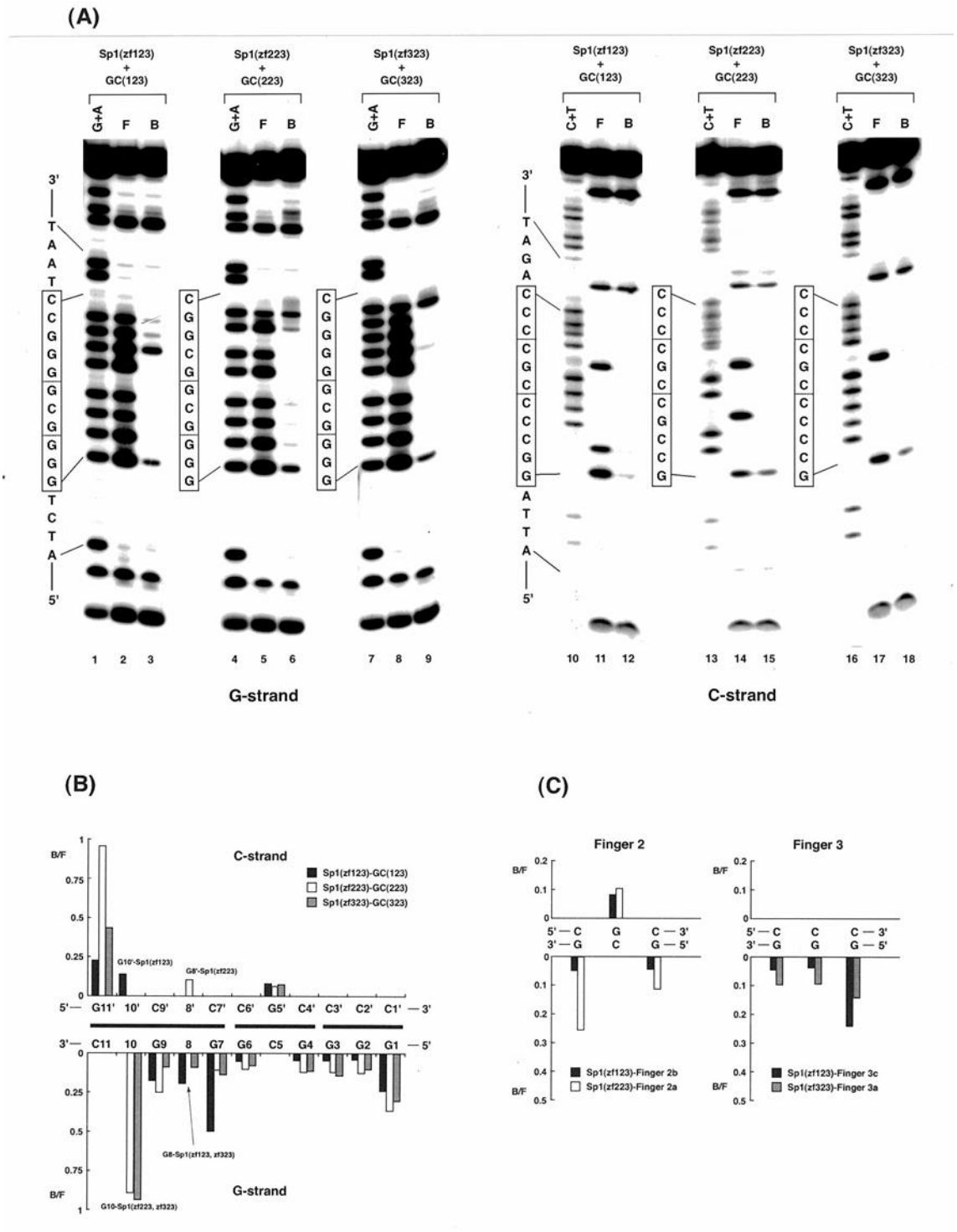
(A)
Sp1(zf123) + GC(123)
Sp1(zf223) + GC(223)
Sp1(zf323) + GC(323)
G+A
C+T
F
B
3'
5'
TAATCCGGGGGCGGGGTCTA
TAGAGCCCCGCGCCCCGATTA
1 2 3 4 5 6 7 8 9
10 11 12 13 14 15 16 17 18
G-strand
C-strand
(B)
C-strand
Sp1(zf123)-GC(123)
Sp1(zf223)-GC(223)
Sp1(zf323)-GC(323)
B/F
G10'-Sp1(zf123)
G8'-Sp1(zf223)
5'— G11' 10' C9' 8' C7' C6' G5' C4' C3' C2' C1' —3'
3'— C11 10 G9 8 G7 G6 C5 G4 G3 G2 G1 —5'
G8-Sp1(zf123, zf323)
G10-Sp1(zf223, zf323)
G-strand
(C)
Finger 2
Finger 3
5'— C G C —3'
3'— G C G —5'
Sp1(zf123)-Finger 2b
Sp1(zf223)-Finger 2a
Sp1(zf123)-Finger 3c
Sp1(zf323)-Finger 3a

Figure 4. (A) Methylation interference analyses for Sp1(zf323) and Sp1(zf321) binding to GC(223) and GC(323). The left and right panels show the results for GC(223) and GC(323), respectively. Lanes 3−10 represent free (F) and bound (B) DNA samples. Lanes 2 and 11 contain G+A and C+T of the Maxam−Gilbert sequencing reactions, respectively. Lanes 1 and 12 show intact DNA. In these experiments, poly(dI-dC) was used as a competitor (see Materials and Methods for details). (B) Histograms showing the extent of methylation interference by Sp1(zf323) and Sp1(zf321) for GC(223) (left) and GC(323) (right). Two or more autoradiograms of the gels were scanned with a densitometer, and the average extent of interference was calculated as the ratio of the cutting probabilities for the two bands (B/F).

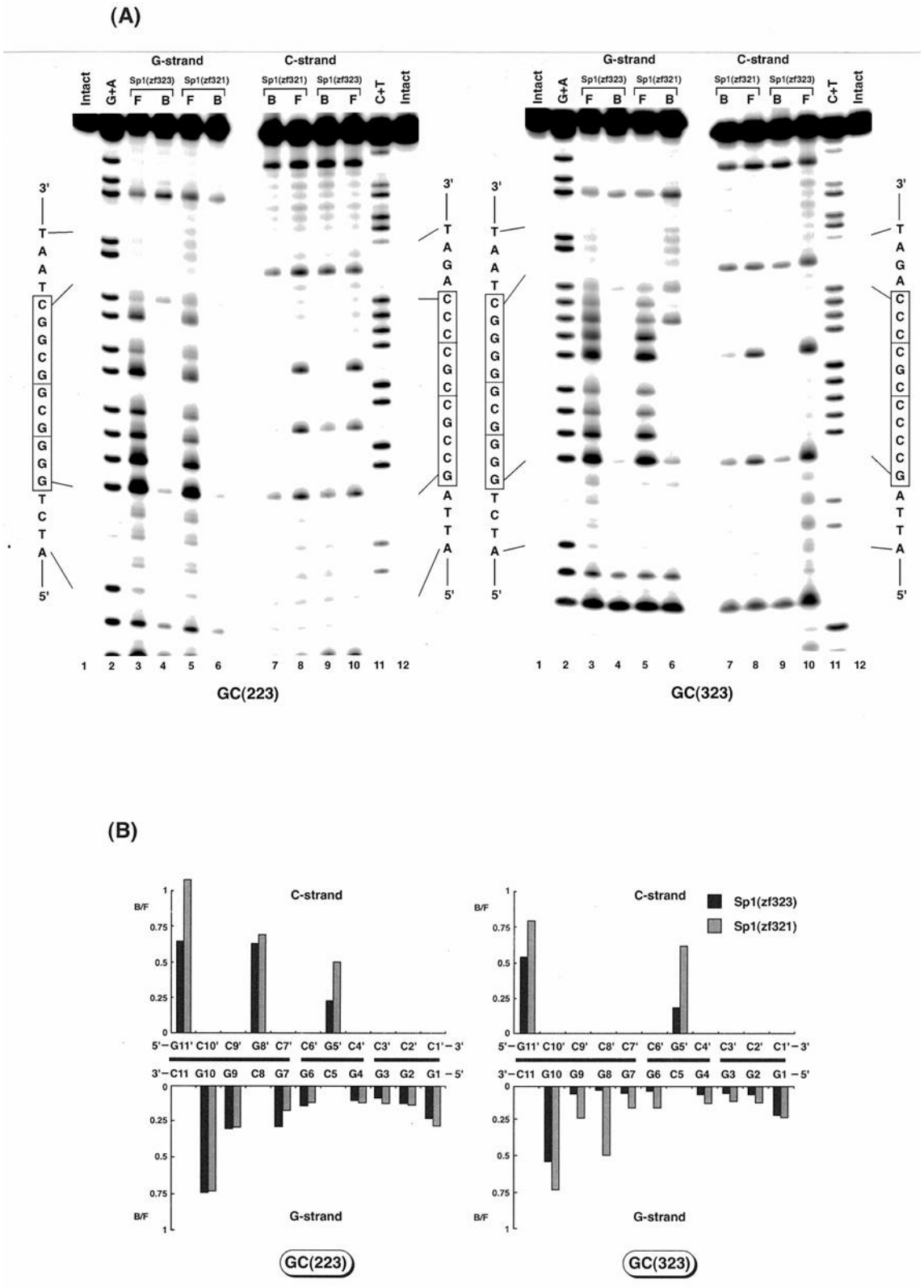
(A)
G-strand
C-strand
Intact
G+A
Sp1(zf323)
Sp1(zf321)
F
B
C+T
3'
5'
GC(223)
GC(323)
(B)
B/F
C-strand
G-strand
Sp1(zf323)
Sp1(zf321)
5'-G11' C10' C9' G8' C7' C6' G5' C4' C3' C2' C1'-3'
3'-C11 G10 G9 C8 G7 G6 C5 G4 G3 G2 G1-5'

Figure 5. DNaseI footprinting analyses for Sp1(zf123), Sp1(zf223), Sp1(zf323), and Sp1(zf321) binding to their high-affinity binding sequence. Panels A and B show the results for the G- and C-strands, respectively. The asterisks represent the enhance sites of cleavage. Lanes 1, 6, 11, 16, and 21 in panel A, G+A (Maxam−Gilbert reaction products); lanes 1, 6, 11, 16, and 21 in panel B, C+T (Maxam−Gilbert reaction products). Peptide concentrations and the combinations of peptide and substrate DNA are noted in the figure

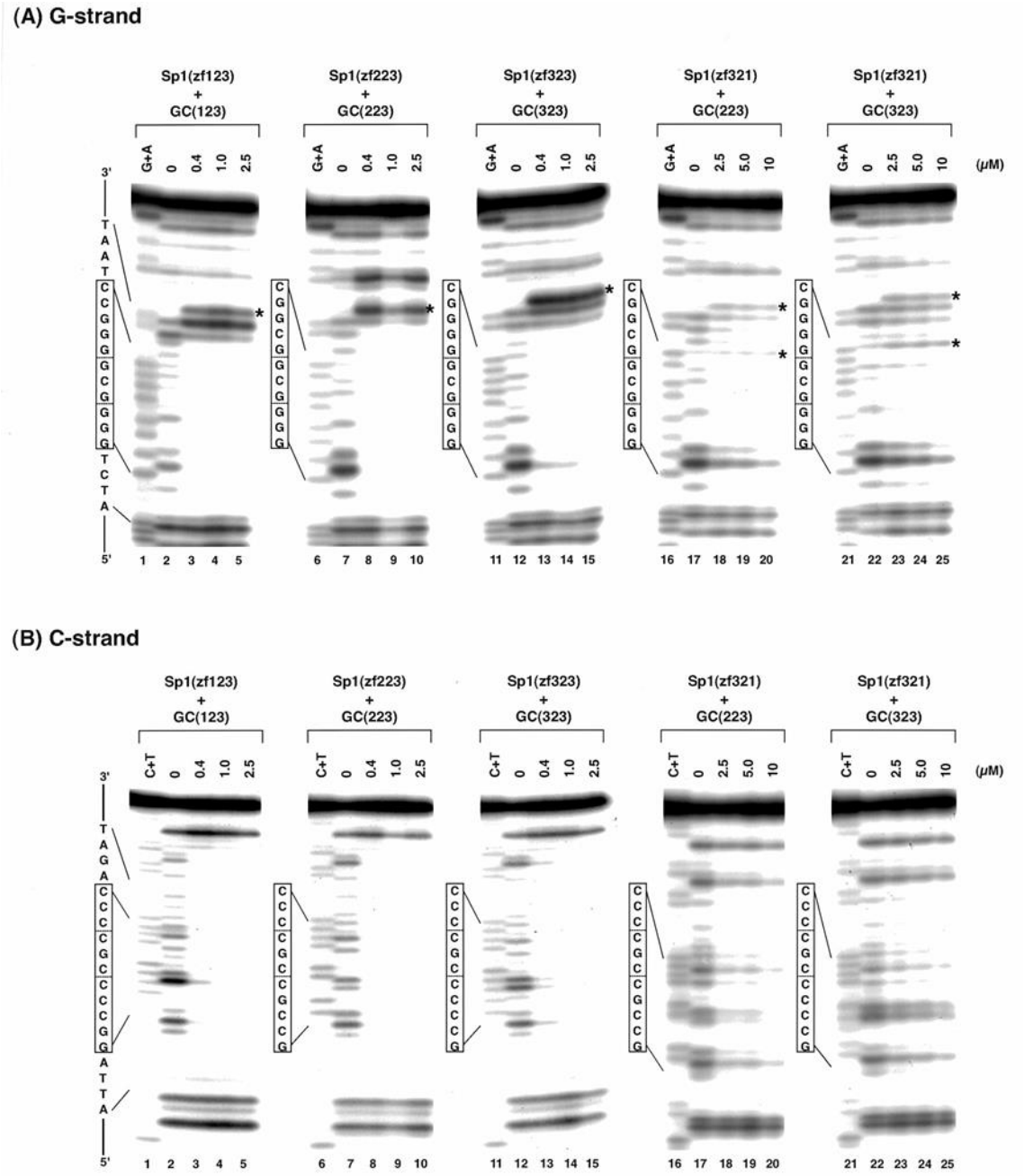
(A) G-strand
Sp1(zf123) + GC(123)
Sp1(zf223) + GC(223)
Sp1(zf323) + GC(323)
Sp1(zf321) + GC(223)
Sp1(zf321) + GC(323)
G+A
0
0.4
1.0
2.5
5.0
10
(μM)
3'
5'
TAATCCGGGGGCGGGGTCTA
1 2 3 4 5
6 7 8 9 10
11 12 13 14 15
16 17 18 19 20
21 22 23 24 25
(B) C-strand
C+T
TAGACCCCCGCCCCCGGATTA

Supplementary Figure 1. DNaseI footprinting analyses for Sp1(zf123), Sp1(zf223), Sp1(zf323), and Sp1(zf321) bindings to GC(123). Left and right panels show the results for the G- and C-strands, respectively. The asterisks represent enhance site of cleavage. Lanes 2, 15, and 16 in left panel, G+A (Maxam-Gilbert reaction products); Lanes 2, 15, and 16 in right panel, C+T (Maxam-Gilbert reaction products). Peptide concentrations are noted in the figure.

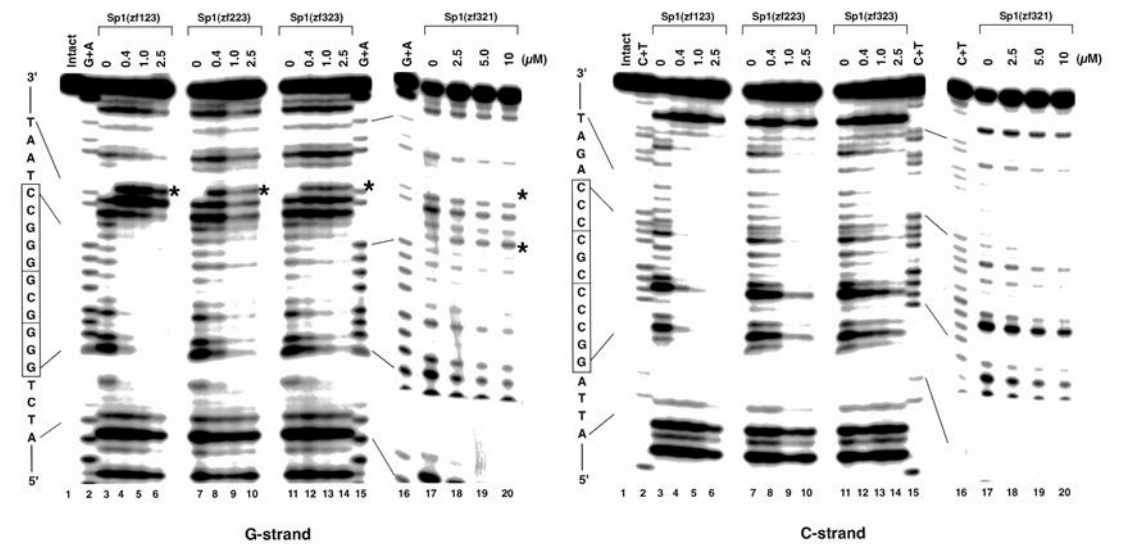
Sp1(zf123)
Sp1(zf223)
Sp1(zf323)
Sp1(zf321)
Intact
G+A
C+T
0
0.4
1.0
2.5
5.0
10
(μM)
3'
5'
TAATCCGGGGCGGGGTCTA
TAGACCCCGCCCCGGATTA
1 2 3 4 5 6 7 8 9 10 11 12 13 14 15 16 17 18 19 20
G-strand
C-strand

Part II

Efficacy of a Novel, Orally Active GSK-3 Inhibitor 6-Methyl-N-[3-[[3-(1-methylethoxy)propyl]carbamoyl] -1H-pyrazol-4-yl]pyridine-3-carboxamide in Tau Transgenic Mice

Abstract

Neurofibrillary tangles (NFTs) composed of hyperphosphorylated and aggregated tau are common pathological characteristics in Alzheimer's disease (AD) and other tauopathies. Aberrant tau phosphorylation is an early and pivotal event in the pathogenesis of tauopathies, and since GSK-3 is a key factor implicated in aberrant tau phosphorylation, GSK-3 inhibition is expected to suppress tauopathy disease progression. In the present study, I report the efficacy of a newly discovered small molecule GSK-3 inhibitor, 6-methyl-N-[3-[[3-(1-methylethoxy)propyl]carbamoyl]-1H-pyrazol-4-yl]pyridine-3-carboxamide (compound **A**), to inhibit tau phosphorylation and to reduce the amount of pathological aggregated tau in JNPL3 mice that overexpress a mutant form of human tau. Compound **A** is a highly potent and selective inhibitor of GSK-3 with an IC_{50} of 2 nM, with at least 230-fold lower potency against 27 other kinases. Oral administration of compound **A** resulted in a significant reduction of tau phosphorylation at several GSK-3 directed sites. Furthermore, chronic oral administration of compound **A** markedly reduced aggregated tau in old JNPL3 mice. These results suggest that a novel, orally active GSK-3 inhibitor, compound **A**, has potency in the prevention of tau pathology.

Introduction

Neurofibrillary tangles (NFTs) composed of hyperphosphorylated and aggregated tau are common pathological characteristics in several neurodegenerative diseases, such as Alzheimer's disease (AD), frontotemporal dementia with parkinsonism linked to chromosome 17 (FTDP-17), Pick's disease, progressive supranuclear palsy, and corticobasal degeneration that are collectively called tauopathies (48, 49). In AD, the temporal and spatial distribution of NFTs correlates well with clinical disease severity (50, 51). Tau is a microtubule-associated protein, and its normal physiological function is to bind and stabilize microtubules (52). Aberrant phosphorylated tau loses its ability to bind to and stabilize microtubules, leading to disruption of the microtubule assembly and deficits in axonal transport (53-56). Considering recent studies reporting age-dependent synaptic deficits, hippocampal degeneration and memory impairment in transgenic mice overexpressing mutant forms of tau (57, 58), strategies targeting tau pathology are attractive for the treatment of AD and other tauopathies.

Previous studies have demonstrated that tau is a substrate of various kinases, such as cyclin dependent kinase 5 (CDK5), mitogen-activated protein kinase (MAPK) and glycogen synthase kinase-3β (GSK-3β) (59-65). Among these kinases, GSK-3β has been reported to be the predominant tau kinase involved in most of the hyperphosphorylated serine/threonine residues in PHF-tau both *in vitro* and *in vivo* (60). Overexpression of GSK-3β in mammalian cells and transgenic mice resulted in tau hyperphosphorylation, microtubule destabilization, and pathological PHF formation (66-68). In addition, a conditional GSK-3β overexpressing transgenic mouse exhibited some phenotypes such as neuronal death in the hippocampus and cognitive deficits (67, 68). Furthermore, active GSK-3β is localized to pretangle neurons, dystrophic neurites and NFTs in AD brains, and a spatial and temporal pattern of increased active GSK-3β

expression coinciding with the progression of NFTs and neurodegeneration has been observed (69, 70). These observations support a major contribution of GSK-3β in the progression of AD and other tauopathies. Several groups have investigated different classes of small molecule GSK-3 inhibitors (71-74), however, there are only a few reports that describe the efficacy of small molecule GSK-3 inhibitors on *in vivo* tau pathology (75, 76).

In the present study, I report the efficacy of a newly discovered small molecule GSK-3 inhibitor 6-methyl-N-[3-[[3-(1-methylethoxy)propyl]carbamoyl]-1H-pyrazol-4-yl]pyridine-3-carboxamide (compound **A**) on tau pathology. Compound **A** is a highly potent and selective GSK-3 inhibitor with oral activity and has a significant inhibitory effect on *in vivo* tau phosphorylation. In addition, chronic administration of compound **A** resulted in a marked reduction of aggregated tau in old JNPL3 mice that overexpress a mutant form of human tau (77).

Materials and Methods

Antibodies

The following antibodies were used for immunoblotting at appropriate concentrations as recommended by the manufacturers. Mouse monoclonal antibodies recognizing phospho-specific epitopes on tau, AT8 for Ser202/Thr205, AT180 for Thr231, and AT270 for Thr181, and human total tau, HT-7, were purchased from Innogenetics (Ghent, Belgium). Rabbit polyclonal antibodies recognizing phospho-specific epitopes on tau, Thr205, Ser262, Ser396, and Ser422 were purchased from Biosource International (Camarillo, CA, USA). Rabbit polyclonal antibody recognizing total tau, Tau Ab-3, was purchased from Lab Vision Corporation (Fremont, CA, USA). Mouse monoclonal antibody recognizing β-actin was purchased from Sigma-Aldrich (St. Louis, MO, USA).

Animals

Male C57BL/6Njcl mice, age 8 weeks, (Clea Japan, Tokyo, Japan) were used for the cold water stress model. Homozygous JNPL3Hlmc mice (Taconic Farms, Germantown, NY, USA) were also used in this report. JNPL3 are transgenic mice that overexpress human 4R0N tau with the FTDP-17 (P301L) mutation (77). All animals were housed in groups and were allowed free access to food and water. All animals used in this study were cared for in accordance with the Principles and Guidelines on Animal Experimentation of the Pharmaceutical Research Division of Takeda Pharmaceutical Company Ltd.

Cold Water Stress (CWS)

CWS (78, 79) was given between 13:00 and 18:00. Thirty min after oral administration of compound **A**, mice were immersed up to the neck in cold water (1-2°C) for 4 min and then were returned to individual cages. Mice were sacrificed by decapitation 30 min after the CWS, the brains were immediately removed, and the hippocampi were dissected.

Drugs and Drug Administration

6-Methyl-N-[3-[[3-(1-methylethoxy)propyl]carbamoyl]-1H-pyrazol-4-yl]pyridine-3-carboxamide (compound **A**) was synthesized in the Pharmaceutical Research Division of Takeda Pharmaceutical Company Ltd. (Osaka, Japan). In the case of the CWS model, compound **A** was suspended in 0.5% methylcellulose and was administered orally in a volume of 10 ml/kg of body weight 30 min before the CWS.

In the JNPL3 study, JNPL3 mice were divided into two matching groups. In the study with female JNPL3 mice, age 5.5 months, compound **A** was suspended in 0.5% methylcellulose at 10 mg/ml and was administered to mice twice daily in a volume of 10 ml/kg of body weight by oral gavage for 1 month. Mice were sacrificed 30 min after the final treatment by decapitation and the brains were immediately removed. One brain hemisphere was frozen in powdered dry ice, and the other half was immediately homogenized in ice-cold radio-immunoprecipitation assay (RIPA) buffer (50 mM Tris-HCl (pH 7.6), 5 mM ethylenediamine tetra acetic acid (EDTA), 1 mM ethylene glycol tetraacetic acid (EGTA), 30 mM NaF, 5 mM sodium diphosphate, 2 μM pepstatin A, 100 mM NaCl, 1% NP-40, 0.25% sodium deoxycholate, 1 μM microcystin LR, 40 μM leupeptin, 100 μM 4-(2-aminoethyl)benzenesulfonyl fluoride (ABSF), 2 mM sodium orthovanadate, 1 μM MG115). In the study with male JNPL3 mice, age 12.5 months, mice were singly housed two weeks before starting treatment, and their basal food intake was measured. Subsequently, mice were treated by feeding with chow containing 200 mg of compound **A** per kg

chow (0.02%) for 1 month. In this dosing paradigm, 26 mg/kg/day of compound **A** were administered to the mice. Mice were sacrificed by decapitation, and tissues were analyzed as described below.

Preparation of Protein Extract

Tissues were immediately homogenized in ice-cold RIPA buffer and centrifuged at 20,000 ×g for 10 min at 4°C. The supernatants were transferred to fresh tubes and were used as the soluble fraction. For analysis of aggregated tau from JNPL3 mice, sarkosyl extraction was performed (80, 81). The pellets were rehomogenized with 0.5 M NaCl containing 10% sucrose and incubated with a final volume of 1% sarkosyl for 1 hour at 37°C. After centrifugation at 256,000 ×g for 15 min, the pellets were resuspended by ultrasonication in phosphate buffered saline, and this suspension was used as the sarkosyl insoluble fraction.

Total protein lysate of AD patient hippocampus was purchased from BioChain Institute, Inc. (Hayward, CA, USA). After centrifugation at 20,000 ×g for 10 min at 4°C, the pellet was used for sarkosyl extraction as described above.

RAB-RIPA-Formic Acid extraction was also performed (82-84). The tissue was homogenized in ice-cold high-salt RAB buffer [0.1 M morpholineethanesulfonic acid (MES), 1 mM EGTA, 0.5 mM $MgSO_4$, 0.75 M NaCl, 0.02 M NaF, 100 μM ABSF and protease inhibitors (Complete Mini, Roche Applied Science, Mannheim, Germany), pH 7.0], and the sample was centrifuged at 50,000 ×g for 20 min at 4°C. The supernatant was boiled for 5 min and then centrifuged at 10,000 ×g for 20 min at 4°C. The resulting supernatant contains the soluble tau fraction (RAB fraction). To remove myelin and associated lipids, the RAB insoluble pellets were reextracted with 1 M sucrose/RAB buffer and centrifuged at 100,000 x g for 30 min at 4°C. The pellets were suspended in RIPA buffer and centrifuged as above and the supernatants were

collected (RIPA fraction). Finally, the RIPA-insoluble pellets were reextracted with 70% formic acid (FA). Protein concentrations were determined using BCA protein assay reagents (PIERCE, Rockford, IL, USA).

SDS-PAGE and Western Blotting

Samples containing 3-10 μg of proteins were separated on a 10% SDS-polyacrylamide gel and were transferred to a polyvinylidene fluoride (PVDF) membrane. The membrane was washed once with 0.1% Tween-20 containing Tris-buffered saline (TBS-T) for 15 min before treatment with Block-Ace (DS Pharma Biomedical, Tokyo, Japan) for 45 min and then was probed with primary antibody in TBS-T containing 3% bovine serum albumin (BSA). The membrane was washed 3 times with TBS-T and then incubated with the anti-mouse or anti-rabbit IgG horseradish peroxidase-linked species-specific $F(ab')_2$ fragment (GE Healthcare, Piscataway, NJ, USA) in TBS-T for 1 hour. After washing 3 times with TBS-T, the blot was developed with ImmunoStar Reagents (Wako Pure Chemical Ind., Osaka, Japan). The images obtained with a CCD camera (LAS-1000plus Luminescent Image Analyzer, Fuji Film, Tokyo, Japan) were quantified by densitometry (Image Gauge Ver. 3.46, Fuji Film).

Preparation and Treatment of Rat Primary Cortical Neuron

Rat primary neuronal cells were prepared from E17 rat fetus (Japan SLC, Hamamatsu, Japan). The cells were suspended in NeuroBasal medium (Invitrogen Life Technologies, Carlsbad, CA) supplemented with B27 supplement (Invitrogen Life Technologies), 0.5 mM glutamine and penicillin-streptomycin. The cells were cultured on poly-L-lysine coated plates (Sumitomo Bakelite, Akita, Japan) under a 5% CO_2 atmosphere at 37°C. The cells were then treated with

compound **A** in 0.1% dimethylsulfoxide (DMSO), and cultured for 2 hours. Following 2 hours of drug treatment, the culture media was removed and the cells were extracted into RIPA buffer.

Immunohistochemistry

After dissection, each brain was frozen in powdered dry ice. Frozen brains were sectioned at 20 μm thickness using a Leica CM-1850 cryomicrotome (Leica Microsystems Nussloch GmbH, Nussloch, Germany) and were mounted onto silane-coated slides. After fixation with Mildform 10 N (Wako Pure Chemical Ind.), slides were washed with TBS containing 1 mM $CaCl_2$ (TBS-Ca), treated with 0.1% Triton X-100 containing TBS-Ca for 30 min, and then treated with 0.6% hydrogen peroxide in methanol for 30 min. After blocking with Block-Ace containing 3% fetal bovine serum, slides were probed with primary antibodies followed with horseradish peroxidase (HRP)-coupled secondary antibodies, detected by 3,3'-diaminobenzidine tetrahydrochloride (DAKO Cytomation, Glostrup, Denmark), and counterstained with hematoxylin. The images were captured using a Nikon Eclipse E800M microscope (Nikon, Tokyo, Japan) and a Nikon Dxm1200 camera (Nikon).

GSK-3 or CDK5 Kinase Assay

The human GSK-3α was purchased from Millipore Corp. (Bedford, MA), which was expressed as an N-terminal 6xHis-tagged protein using a baculovirus expression system. Human GSK-3β was expressed as an N-terminal FLAG-tagged protein using a baculovirus expression system (Takeda Pharmaceutical Company Ltd., Osaka, Japan). Human p35/cyclin dependent kinase 5 (CDK5) was purchased from Millipore Corp., which was expressed as an N-terminal GST fusion protein using a baculovirus expression system. The kinase assay was performed in a reaction mixture that contained 25 mM HEPES, pH 7.5, 10 mM magnesium acetate, 1 mM

dithiothreitol, and 0.01% BSA and serially diluted test compounds. The assay was done in a 96-well plate assay format. The final amount of enzyme and substrate were optimized for each kinase: GSK-3α (40 ng/well of enzyme, 400 ng/well of GSK-3 substrate peptide (Millipore Corp.)); GSK-3β (40 ng/well of enzyme, 100 ng/well of GSK-3β substrate peptide (Millipore Corp.)); CDK5 (20 ng/well of enzyme, 1 ng/well of CDK5 substrate peptide (Calbiochem, La Jolla, CA)).

All the kinase reactions were started by addition of the ATP solution (final 500 nM), and were incubated for 45 min at room temperature for GSK-3α or 90 min at 37 °C for GSK-3β or for 45 min at room temperature for CDK5. The reactions were terminated by the Kinase-Glo reagent containing EDTA (50 μl/well, Promega Corp., Madison, WI). Ten minutes after addition of the Kinase-Glo reagent, luminescence was measured on a Wallac ARVO 1420 (PerkinElmer, Shelton, CT). The reaction window was calculated from the difference of the average signals obtained from the control (5% DMSO) and the background wells. The compound inhibition was expressed as the inhibitor concentration that produced 50% inhibition (IC_{50}) of the activity without compound. The IC_{50} values were obtained by linear regression analysis with a GraphPad Prism (version 3.02 for Windows, GraphPad Software, Inc., San Diego, CA). The best fit lines were obtained by analyzing the logistic fitting equation.

Serine/threonine Kinase Profiling by IC_{50} Measurement

Assays for 14 serine/threonine kinases using radio labeled [γ-^{33}P] ATP (GE Healthcare, Piscataway, NJ) were performed in 96 well plates. Mitogen-activated protein kinase p38 alpha (p38α), extracellular signal-regulated kinase 1 (ERK1), protein kinase C theta (PKCθ), Jun N-terminal kinase 1 (JNK1) and B-raf were expressed as N-terminal FLAG tagged proteins using a baculovirus expression system. I kappa B kinase β (IKKβ) and MEK kinase 1 (MEKK1) were

expressed as C-terminal FLAG tagged proteins using a baculovirus expression system. Aurora-B was expressed as N-terminal 6xHis tagged protein using a baculovirus expression system. MEK1 was expressed as N-terminal GST fusion protein using a freestyle293 (Invitrogen Life Technologies) expression system. Cyclic AMP-dependent protein kinase (PKA) was expressed using an *Escherichia coli* (*E.coli*) expression system. Casein kinase 1 delta (CK1δ) was expressed as an N-terminal GST fusion protein using an E.coli expression system. Checkpoint kinase 1 (CHK1) was expressed as an N-terminal GST fusion protein using a baculovirus expression system. CDK1/CycB and CDK2/CycA were expressed as C-terminal 6xHis-tagged CDK1 or CDK2, and N-terminal GST-tagged Cyclin B or Cyclin A proteins using a baculovirus expression system.

The reaction conditions were optimized for each kinase: p38α (100 ng/well of enzyme, 1 μg/well of myelin basic protein (MBP) (Wako pure chemical Ind.), 0.1 μCi/well of [γ-^{33}P] ATP, 60 min reaction at 30°C); ERK1 (100 ng/well of enzyme, 2 μg/well of MBP, 0.1 μCi/well of [γ-^{33}P] ATP, 60 min reaction at 30°C); MEKK1 (25 ng/well of enzyme, 1 μg/well of MBP, 0.1 μCi/well of [γ-^{33}P] ATP, 60 min reaction at 30°C); PKCθ (25 ng/well of enzyme, 2 μg/well of MBP, 0.1 μCi/well of [γ-^{33}P] ATP, 60 min reaction at 30°C); JNK1 (10 ng/well of enzyme, 1 μg/well of c-Jun, 0.1 μCi/well of [γ-^{33}P] ATP, 60 min reaction at 30°C); IKKβ (20 ng/well of enzyme, 1 μg/well of IκBα, 0.1 μCi/well of [γ-^{33}P] ATP, reaction at room temperature); B-raf (25 ng/well of enzyme, 1 μg/well of GST-MEK1(K96R), 0.1 μCi/well of [γ-^{33}P] ATP, 20 min reaction at room temperature); MEK1 (100 ng/well of enzyme, 0.3 μg/well of GST-ERK1 (K71A) 0.2 μCi/well of [γ-^{33}P] ATP, 20 min reaction at room temperature); Aurora-B (50 ng/well of enzyme, 30 μM of Aurora substrate peptide, 0.2 μCi/well of [γ-^{33}P] ATP, 60 min reaction at room temperature); PKA (3 nM of enzyme, 1 μM of PKA substrate peptide (Millipore, Corp.), 0.2 μCi/well of [γ-^{33}P] ATP, 10 min reaction at room temperature); CDK1/CycB (4.2 ng/well of

enzyme, 1 μg/well of Histone H1 (Calbiochem), 0.2 μCi/well of [γ-^{33}P] ATP, 20 min reaction at room temperature); CDK2/CycA (1.8 mUnits/well of enzyme, 1 μg/well of Histone H1, 0.2 μCi/well of [γ-^{33}P] ATP, 20 min reaction at room temperature); CK1δ (120 ng/well of enzyme, 2.4 μM of CK1tide (Millipore Corp.), 0.2 μCi/well of [γ-^{33}P] ATP, 20 min reaction at room temperature); CHK1 (30 ng/well of enzyme, 25 μM of CHKtide (Millipore Corp.), 0.2 μCi/well of [γ-^{33}P] ATP, 10 min reaction at room temperature).

Except for the PKCθ, enzyme reactions were performed in 25 mM HEPES, pH 7.5, with 10 mM magnesium acetate, 1 mM dithiothreitol and 500 nM ATP containing an optimized concentration of enzyme, substrate and radiolabeled ATP as described above in a total volume of 50 μl. For PKCθ, enzyme reactions were performed in 25 mM HEPES, pH 7.5, with 10 mM magnesium acetate, 1 mM dithiothreitol, and lipid activator (Millipore Corp.).

Prior to the kinase reaction, compound and enzyme were incubated for 5 min at the reaction temperature as described above. The kinase reactions were initiated by the addition of ATP. After the reaction period as described above, the reactions were terminated by the addition of 10% trichloroacetic acid (final concentration). The [γ-^{33}P]-phosphorylated proteins were filtered in a Harvest Plate (Millipore Corp.) with a Cell Harvester (PerkinElmer) and then free [γ-^{33}P] ATP was washed out with 3% phosphoric acid. The plates were dried, followed by the addition of 40 μl of MicroScint0 (PerkinElmer). The radioactivity was counted by a TopCount scintillation counter (PerkinElmer).

Tyrosine Kinase Profiling by IC_{50} Measurement

The cytoplasmic domain of vascular endothelial growth factor receptor 2 (VEGFR2) was expressed as an N-terminal FLAG-tagged protein using the baculovirus expression system. The cytoplasmic domains of v-erb-a erythroblastic leukemia viral oncogene homolog 2 (ERBB2)

and epidermal growth factor receptor (EGFR) were expressed as N-terminal peptide (DYKDDDD)-tagged proteins using a baculovirus expression system. These expressed kinase proteins were purified using an anti-FLAG M2 affinity gel (Sigma-Aldrich). Fibroblast growth factor receptor 3 (FGFR3), platelet-derived growth factor receptor alpha (PDGFRα), PDGFRβ, TIE2, c-Met, c-Kit, Src, insulin receptor (IR), and lymphocyte-specific protein tyrosine kinase (Lck) were purchased from Millipore Corp.

Assays for 10 tyrosine kinases, except ERBB2 and EGFR, using anti-phosphotyrosine antibodies were performed in 384 well plates using the Alphascreen® system (PerkinElmer) at room temperature. Enzyme reactions were performed in 50 mM Tris-HCl, pH 7.5, containing 5 mM $MnCl_2$, 5 mM $MgCl_2$, 0.01% Tween-20, 2 mM dithiothreitol, 0.1 μg/ml biotinylated poly-GluTyr (4:1) and optimized concentrations of enzyme and ATP as described below.

Prior to the kinase reaction, compound and enzyme were incubated for 5 min at room temperature. The reactions were initiated by the addition of ATP. After the reaction period (described below), the reactions were stopped by the addition of 25 μl of 100 mM EDTA, 10 μg/ml Alphascreen streptavidine donor beads and 10 μg/ml acceptor beads (described below) in 62.5 mM HEPES, pH 7.4, 250 mM NaCl, and 0.1% BSA. The plates were incubated in the dark for more than 12 hours and then read by an EnVision 2102 Multilabel Reader (PerkinElmer). The well containing substrate and enzyme without compound was used as a total reaction control. The reaction conditions for these 10 kinases were optimized for each kinase: VEGFR2 (19 ng/ml of enzyme, 10 μM ATP, 10 min reaction, PY-100 conjugated acceptor beads (PY-100)); FGFR3 (20 ng/ml of enzyme, 20 μM ATP, 10 min reaction, PY-100); PDGFRα (50 ng/ml of enzyme, 10 μM ATP, 30 min reaction, PT66 conjugated acceptor beads (PT66)); PDGFRβ (50 ng/ml of enzyme, 20 μM ATP, 60 min reaction, PT66); TIE2 (20 ng/ml of enzyme, 2 μM ATP, 10 min reaction, PT66); c-Met (1 ng/ml of enzyme, 2 μM ATP, 10 min reaction, PT66); c-Kit (10 ng/ml of enzyme,

20 μM ATP, 20 min reaction, PT66); Src (0.33 ng/ml of enzyme, 2 μM ATP, 10 min reaction, PY-100); IR (100 ng/ml of enzyme, 10 μM ATP, 60 min reaction, PT66); Lck (100 ng/ml of enzyme, 2 μM ATP, 30 min reaction, PY-100).

Assays for ERBB2 and EGFR kinases using radiolabeled [γ-^{32}P] ATP (GE Healthcare) were performed in 96 well plates. ERBB2 and EGFR kinase reactions were performed in 50 mM Tris-HCl, pH 7.5, 5 mM $MnCl_2$, 0.01% Tween-20 and 2 mM dithiothreitol containing 0.9 μCi of [γ-^{32}P] ATP per reaction, 50 μM ATP, 5 μg/ml poly-Glu-Tyr (4:1), 0.1% DMSO and 0.25 μg/ml of ERBB2 or EGFR cytoplasmic domains in a total volume of 50 μl. Prior to the kinase reaction, compound and enzyme were incubated for 5 min at room temperature. The kinase reactions were initiated by the addition of ATP. After the kinase reacted for 10 minutes (ERBB2) and 5 minutes (EGFR) at room temperature, the reactions were terminated by the addition of 10% trichloroacetic acid (final concentration). The [γ-^{32}P]-phosphorylated proteins were filtered in a Harvest plate (Millipore Corp.) with a Cell harvester (PerkinElmer) and were washed free of [γ-^{32}P] ATP with 3% phosphoric acid. The plate was dried, followed by the addition of 25 μl of MicroScint0 (PerkinElmer). The radioactivity was counted by a TopCount scintillation counter (PerkinElmer).

Plasma and Brain Exposure Measurement

Compound **A** was administered to non-fasted C57BL/6N mice (male, 8 weeks old, n= 3) orally (10 mg/kg, 0.5% methylcellulose suspension). At 30, 60 and 120 minutes after oral administration, blood and brain (hippocampus, cerebral cortex, and celleberum) samples were collected. The blood samples were centrifuged to obtain the plasma fraction. The brain samples were homogenized in saline to obtain the brain homogenate. The plasma and brain homogenate samples were deproteinized with acetonitrile containing an internal standard. After centrifugation, the supernatants were decanted into microplates, and were diluted with 0.01 mol/L ammonium

formate and acetonitrile (7/3, v/v) containing 0.2% formic acid. After another centrifugation, the supernatants were injected into a LC/MS/MS system to measure the compound concentrations.

Statistical Analyses

Statistical analysis was performed by statistical analysis software (SAS pre-clinical package, version 5.0; SAS Institute, Inc., Cary, NC). Values were expressed as mean ± S.E.M. and statistically analyzed by using unpaired Student's t-test or one-tailed Williams' test, which is a suitable test for a dose dependent study.

Results

Novel GSK-3 Inhibitor compound A

In the search for novel GSK-3 inhibitors, compound **A** was selected for further study on the basis of its enzyme inhibition, pharmacokinetics, and tau phosphorylation assay results in primary neuronal cells. The chemical structure of compound **A** is shown in Figure 6. Compound **A** inhibited GSK-3α with an IC_{50} value of 2.3 nM and GSK-3β with an IC_{50} value of 2.0 nM in the presence of 500 nM ATP. In order to assess the selectivity of compound **A**, I measured its inhibitory potency against a number of serine/threonine and tyrosine kinases (Table 2). This compound had no inhibitory effect on 23 kinases including extracellular signal-regulated kinase 1 (ERK1), cAMP-dependent protein kinase (PKA) and p38α, and only weak inhibition was detected against CDK1/CycB, CDK2/CycA, CDK5 and Jun N-terminal kinase (JNK) 1 with IC_{50} values of 2, 0.46, 5, and 5.8 μM, respectively. Compound **A** markedly inhibited tau phosphorylation in rat primary neuronal cells, indicating it has good cell membrane permeability. Compound **A** treatment resulted in a reduction of tau phosphorylation at GSK-3 directed sites as detected by AT8 (pSer202/pThr205), AT180 (pThr231), AT270 (pThr181), pThr205 and pSer396 antibodies in a concentration dependent manner with IC_{50} values of 1.9, 0.44, 24, 0.25, and 5.2 μM, respectively (Figure 7). Compound **A** did not reduce tau phosphorylation at GSK-3 non-directed pSer262 and pSer422 sites and also did not affect the amount of total tau. These results suggest that compound **A** reduces tau phosphorylation in primary neuronal cells thorough GSK-3 inhibition.

Effect of Compound A on Tau Phosphorylation in a Cold Water Stress Model

Some previous reports have indicated that cold water stress (CWS) transiently induces *in vivo* tau hyperphosphorylation, and a single intraperitoneal administration of the GSK-3 inhibitor lithium chloride (LiCl) inhibited CWS-induced tau hyperphosphorylation (78, 79). I used the CWS model to evaluate the *in vivo* efficacy of the novel GSK-3 inhibitor compound **A** on tau phosphorylation. The concentrations of Compound **A** measured in plasma, hippocampus, cerebral cortex, and cerebellum after 30, 60, and 120 min are summarized in Table 3. Compound **A** was suspended in 0.5% methylcellulose and was administered orally 30 min before CWS at a dose of 1-10 mg/kg. As indicated in Figure 8, compound **A** significantly inhibited tau phosphorylation in a dose dependent manner as detected by the pThr205 antibody. 10 mg/kg of compound **A** reduced tau phosphorylation to the level of the CWS non-treated control group. Compound **A** displayed a highly potent inhibition of *in vivo* tau phosphorylation in the CWS model.

Evaluation of Compound A Efficacy in JNPL3 Mice Expressing Human Tau

I then investigated the ability of compound **A** to inhibit tau hyperphosphorylation and tau aggregation in a JNPL3 mouse model. JNPL3 mice are well characterized transgenic mice that express human 4R0N tau with a FTDP-17 (P301L) mutation. Their phenotype mimics features of human tauopathies (77); in particular, the levels of sarkosyl insoluble tau in JNPL3 mice increase in an age dependent manner and co-migrate with insoluble tau from AD and FTDP-17 brains. Thus, JNPL3 mice are a useful model to evaluate tau targeting agents for the treatment of AD or other tauopathies.

Initially, I treated homozygous female JNPL3 mice at age 5.5 months with compound **A** for 1 month. It was previously reported that a significant amount of sarkosyl insoluble tau was detected in brain tissue from JNPL3 mice of this approximate age (77). From the results of the

CWS model and the pharmacokinetic profile, I determined a dose for compound **A** of 10 mg/kg twice daily by oral gavage. There was no significant reduction of body weight in the compound **A** treated group as compared with the vehicle treated group (data not shown). Compound **A** treatment resulted in a significant reduction of tau phosphorylation at GSK-3 directed sites as detected by pThr205, pSer396, AT8, AT180 and AT270 antibodies in the soluble tau fraction (Figure 9A, B). Consistent with the results in primary neurons, the most striking reduction was seen at the AT180 (pThr231) sites. As for GSK-3 non-directed pSer262 and pSer422 sites, compound **A** did not significantly reduce tau phosphorylation. I then investigated the effect of compound **A** on aggregated, sarkosyl insoluble tau that was biochemically similar to NFTs. Compound **A** treatment resulted in a 49%, 66%, and 58% reduction of sarkosyl insoluble tau detected by total tau, pThr205, and HT7 antibodies, respectively (Figure 9C, D); however, these reductions were not significant due to the variability in the amounts of sarkosyl insoluble tau in JNPL3 mice. I also conducted immunohistochemical analyses. Phosphorylated tau signals detected by a pThr205 antibody were markedly decreased by compound **A** treatment especially at CA1, CA3, and dentate gyrus regions (Figure 10A-H). Human tau specific signals detected by HT-7 were also reduced in compound **A** treated mice brains (Figure 10I-P). Since compound **A** did not affect the amounts of the soluble fractions of total tau and aggregated tau was mainly composed of transgenic human tau in JNPL3 mice brains (77), these results indicate that compound **A** treated mice had reduced levels of aggregated tau.

I next examined the ability of compound **A** to prevent later stage tau pathology by using much older JNPL3 mice (12.5 months old). As determined from my preliminary study that the amounts of tau protein in aged male JNPL3 mice varied less than in female mice, I used male mice for this experiment. In this experiment, 26 mg/kg/day of compound **A** was administered to mice for 1 month by feeding, with no significant changes observed in food intake and body weight

as compared to the control group (Supplemental Figure 2). Immunohistochemical analyses revealed that pThr205 and HT-7 signals were strikingly diminished by compound **A** treatment (Figure 11). Compound **A** treatment also showed a significant reduction of sarkosyl insoluble tau (total tau, -60%; pThr205, -61%; HT7, -66%) (Figure 12). I have also determined a significant effect of compound **A** on insoluble tau extracted by another procedure (RAB-RIPA-FA extraction, Supplemental Figure 3). Thus, chronic oral treatment of the novel GSK-3 inhibitor compound **A** led to a robust reduction of pathological aggregated tau at a later stage of tau pathology.

Discussion

NFTs composed of hyperphosphorylated, aggregated tau are a common hallmark of tauopathies, such as Alzheimer's disease and FTDP-17. Since abnormal tau phosphorylation is considered to be an early and pivotal event in the pathogenesis of tauopathies and GSK-3 is a key factor in aberrant tau phosphorylation, GSK-3 inhibition is expected to mitigate disease progression in tauopathies. Indeed, some groups have already demonstrated the ameliorating effects of lithium, used as a treatment of mood disorder for many years, on tauopathies (75, 85-87). Several classes of small molecule GSK-3 inhibitors have already been developed (71-74); however, there are few reports describing the *in vivo* efficacy of these compounds on tau pathology (75, 76, 88). In the current report, I investigate the *in vitro*/*in vivo* efficacy of a recently discovered, novel GSK-3 inhibitor, compound **A,** to inhibit tau phosphorylation and aggregated tau.

Compound **A** is selective for GSK-3 with an IC_{50} of 2 nM and 230-fold lower potencies for 27 other kinases. Compound **A** has been found to be one of the most potent and selective GSK-3 inhibitors as compared to previously reported compounds (71, 77, 88) and shows inhibitory effects on tau phosphorylation at GSK-3 directed sites in primary neuronal cells and mouse brain tissue. Yoshida *et al*. reported that intraperitoneal administration of 300 mg/kg of LiCl led to a partial suppression of CWS induced tau phosphorylation (79), while in the current study I found that 10 mg/kg of compound **A** completely inhibited CWS induced tau phosphorylation. As compound **A** is an orally active GSK-3 inhibitor with high potency and selectivity, it should be a useful tool in examining the possibility of selective GSK-3 inhibition as a tauopathy treatment.

In the soluble tau fraction from JNPL3 mice, compound **A** reduced phosphorylation among all examined phosphorylation sites most robustly at the Thr231 residue. This result indicates that the Thr231 site is mainly phosphorylated by GSK-3 *in vivo*, and it has been reported that in AD brains pThr231 signals were detected in the earliest stages of tau pathology preceding NFT formation (89, 90). Accordingly, GSK-3 may play an important role in the onset of tauopathies by phosphorylating the Thr231 residue. Since GSK-3 has been shown to phosphorylate tau at most sites in PHF-tau, GSK-3 inhibition would be anticipated to reduce tau phosphorylation at multiple sites. My results indicate that GSK-3 inhibition by compound **A** led to a significant reduction of tau phosphorylation at several GSK-3 directed sites. Meanwhile, Steinhilb *et al*. reported that phosphorylation of a group of serine-proline/threonine-proline sites plays a fundamental role in tau-mediated toxicity in a tau transgenic Drosophila model (91). They also revealed that no single phosphorylation residue plays a dominant role in tau-mediated toxicity, which suggests that multiple sites work together to promote neurodegeneration (92). These data indicate that GSK-3 inhibitors have the potential of delaying the onset and halting the progression of tau pathologies by inhibiting tau phosphorylation at multiple sites.

Chronic administration of compound **A** significantly reduced sarkosyl-insoluble tau in old homozygous JNPL3 mice (12.5 months old). In contrast, chronic administration of lithium failed to reduce sarkosyl-insoluble tau in old heterozygous JNPL3 mice (12 months old) (75) or pre-formed NFTs in FTDP-17 tau / GSK-3β transgenic mice (87). Considering the *in vitro* activity and the results from the CWS model (79), I speculate that these results are mainly due to the weak inhibitory activity of lithium against GSK-3. To my knowledge, this report is the first to show that administration of a GSK-3 inhibitor reduced sarkosyl-insoluble tau in old tau transgenic mice, which suggests that chronic inhibition of GSK-3 by a highly potent and selective inhibitor has the possibility of preventing NFT formation even in a later stage of tau pathology. Although the role

of NFTs in disease progression has not yet been fully elucidated, NFTs are thought to play a crucial role in the disease progression of AD and other tauopathies based on studies with postmortem brains of AD patients that demonstrate the number of NFTs correlates well with the degree of cognitive impairment (50, 51). It is plausible that intracellularly accumulated NFTs of relatively large size directly exert toxic effects on cells and contribute to tauopathy disease progression. Thus, the efficacy of compound **A** toward reducing sarkosyl-insoluble tau in old JNPL3 mice is a significant result.

In summary, I have demonstrated the efficacy of the novel, potent, selective, orally active GSK-3 inhibitor compound **A** for significantly reducing tau phosphorylation and aggregated tau. Chronic administration of compound **A** led to a significant reduction of aggregated tau in old JNPL3 mice brains. Further research on compound **A** and related compounds as a tauopathy treatment will be needed to clarify their efficacy on neurodegeneration and cognitive impairment especially in the later stages of disease.

Tables and Figures

Table 2. Kinase selectivity of compound **A**

Ser/Thr Kinase	IC_{50} (M) of compound **A**	Tyr Kinase	IC_{50} (M) of compound **A**
GSK-3α	2.3E-09	EGFR	>1.0E-05
GSK-3β	2.0E-09	ERBB2	>1.0E-05
CDK5	5.0E-06	Src	>1.0E-05
AuroraB	>1.0E-05	Lck	>1.0E-05
MEK1	>1.0E-05	IR	>1.0E-05
B-raf	>1.0E-05	TIE2	>1.0E-05
ERK1	>1.0E-05	c-Kit	>1.0E-05
PKA	>1.0E-05	c-Met	>1.0E-05
CDK1/CycB	2.0E-06	VEGFR2	>1.0E-05
CDK2/CycA	4.6E-07	FGFR3	>1.0E-05
CHK1	>1.0E-05	PDGFRα	>1.0E-05
p38α	>1.0E-05	PDGFRβ	>1.0E-05
JNK1	5.8E-06		
IKKβ	>1.0E-05		
MEKK1	>1.0E-05		
PKCθ	>1.0E-05		
CK1δ	>1.0E-05		

Table 3. Concentration of compound **A** in mouse plasma, hippocampus, cerebral cortex, and cerebellum after oral administraton at a dose of 10 mg/kg. Determination of concentration of compound **A** was performed as described in the Experimental Procedure.

Time after administration (hr)	Concentration of Compound **A** (μM, n = 3, mean ±SEM)			
	Plasma	Hippocampus	Cerebral cortex	Cerebellum
0.5	1.45 ± 0.06	0.66 ± 0.13	0.48 ± 0.04	0.39 ± 0.03
1	0.20 ± 0.01	0.19 ± 0.02	0.16 ± 0.02	0.14 ± 0.01
2	0.04 ± 0.02	0.08 ± 0.02	0.05 ± 0.01	0.04 ± 0.02

Figure 6. Chemical structure of novel GSK-3 inhibitor compound **A**.

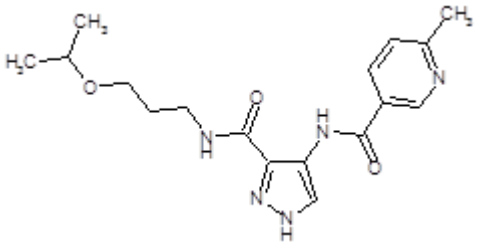

Figure 7. Compound **A** reduced tau phosphorylation in rat primary cortical neurons in a concentration dependent manner. Rat primary cortical neurons at DIV4 were treated with compound **A** at 0.03-30 μM for 2 hours. Cells were extracted and analyzed by immunoblot with phosphorylated tau antibodies: AT8, AT180 and AT270 and total tau antibody.

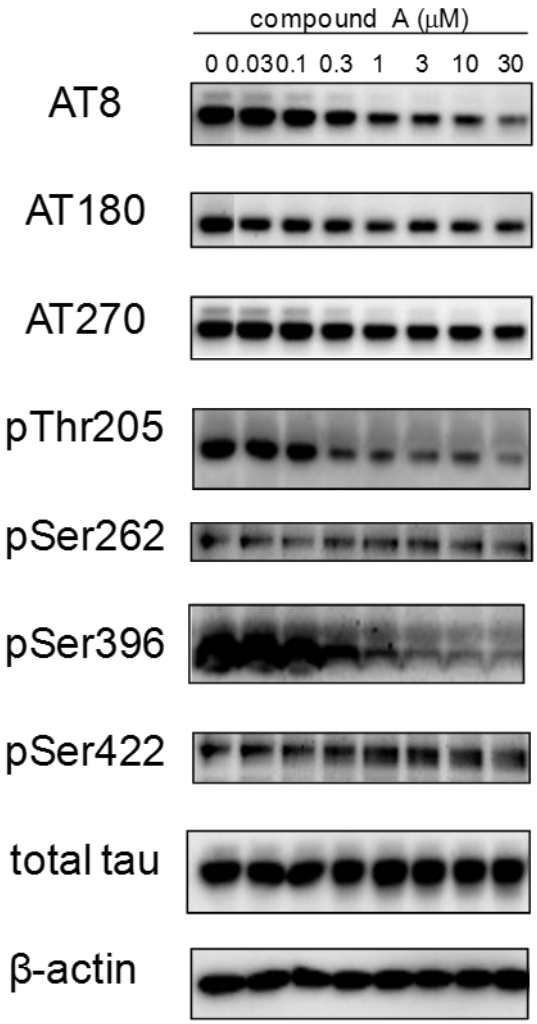
compound A (μM)
0 0.03 0.1 0.3 1 3 10 30
AT8
AT180
AT270
pThr205
pSer262
pSer396
pSer422
total tau
β-actin

Figure 8. Effect of compound **A** on cold water stress (CWS) induced tau phosphorylation. Compound **A** was administered orally at a dose of 1-10 mg/kg 30 min before the CWS. 0.5% methylcellulose was administered to mice as a vehicle treated control. Mice were subjected to CWS for 4 min and sacrificed 30 min after CWS. *A*, Proteins from CWS treated mice hippocampus were separated by SDS-PAGE and detected by pThr205 and total tau antibodies. *B*, Immunoblot bands were quantified by densitometry. Data represent means ± S.E.M. of 5 animals and are expressed as phospho-tau normalized to total tau. Significance is defined as *** $p \leq 0.001$ (*t*-test) in comparison to the non-stressed group and as + $p \leq 0.025$ (Williams' test) in comparison to the vehicle administered group.

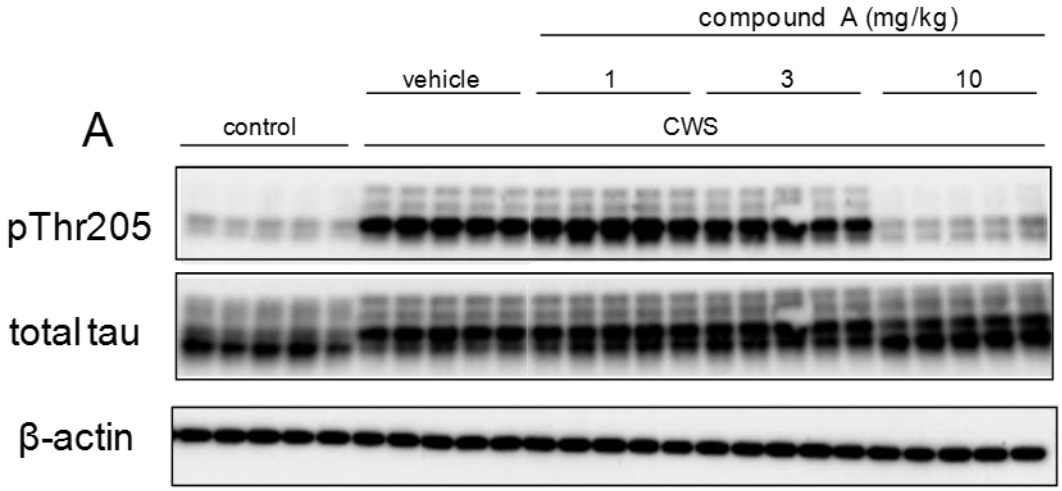
A
compound A (mg/kg)
vehicle
1
3
10
control
CWS
pThr205
total tau
β-actin

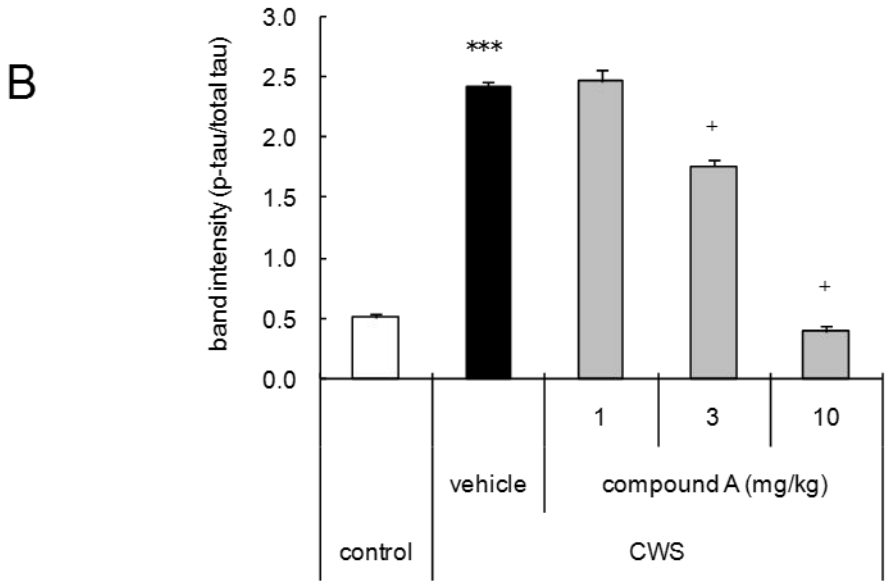
B
band intensity (p-tau/total tau)
3.0
2.5
2.0
1.5
1.0
0.5
0.0
***
+
+
1
3
10
vehicle
compound A (mg/kg)
control
CWS

Figure 9. Effects of compound **A** on tau phosphorylation and aggregated tau in JNPL3 mice brain. Compound **A** was administered at a dose of 10 mg/kg twice daily by oral gavage for 1 month to female JNPL3 mice (5.5 months old). *A*, Proteins from the RIPA soluble fractions of JNPL3 mice hemispheres were separated by SDS-PAGE and detected by pThr205, pSer262, pSer396, pSer422, AT8, AT180, AT270 and total tau antibodies. *B*, Immunoblot bands were quantified by densitometry. Data represent means ± S.E.M. of 10 animals and are expressed as phospho-tau normalized to total tau. Significance is defined as * $p \leq 0.05$, ** $p \leq 0.01$ and *** $p \leq 0.001$ (*t*-test) in comparison to the vehicle administered group. *C*, Proteins from sarkosyl insoluble fractions were separated by SDS-PAGE and detected by total tau, pThr205, and HT7 antibodies. *D*, Immunoblot bands were quantified by densitometry. Data represent means ± S.E.M. of 10 animals.

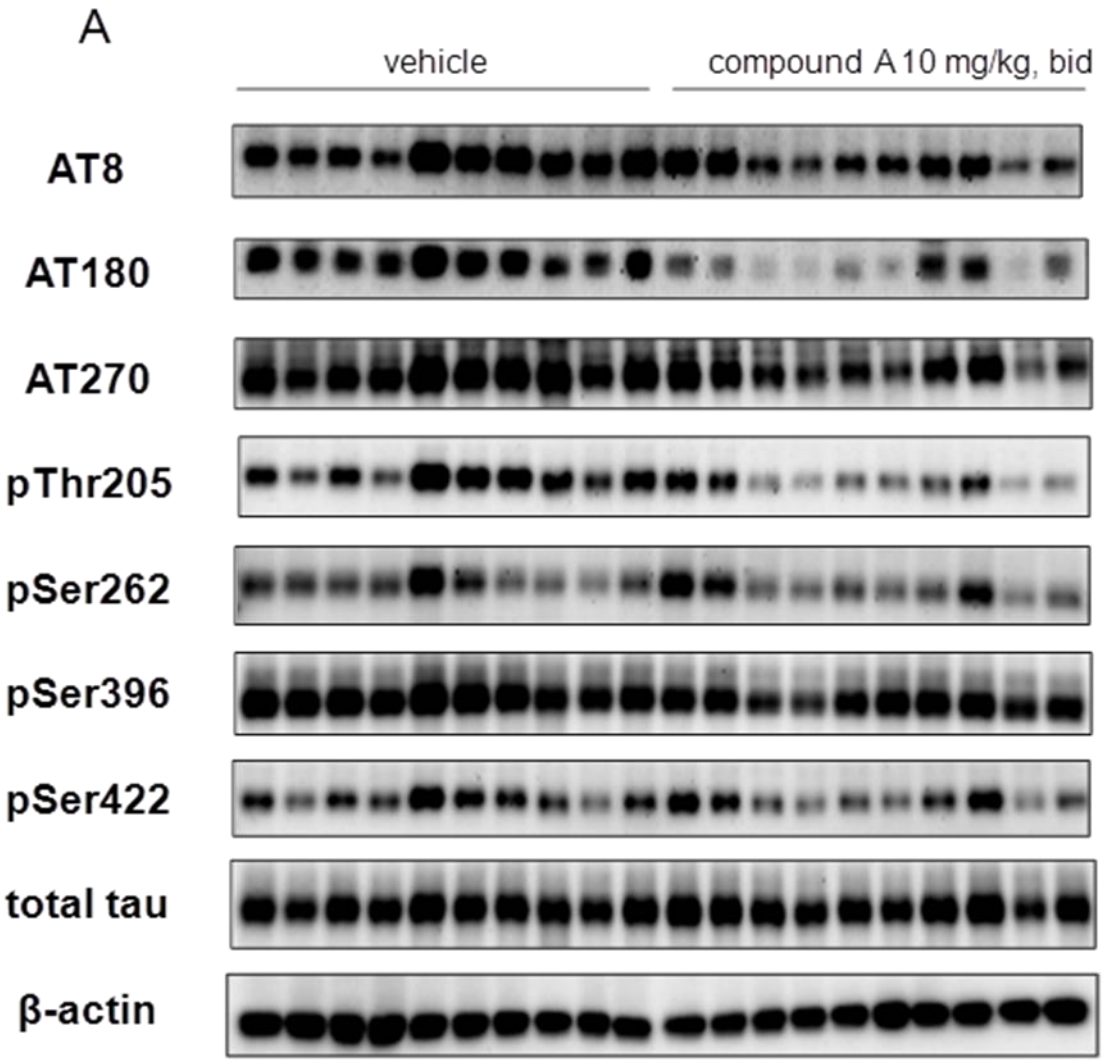
A
vehicle
compound A 10 mg/kg, bid
AT8
AT180
AT270
pThr205
pSer262
pSer396
pSer422
total tau
β-actin

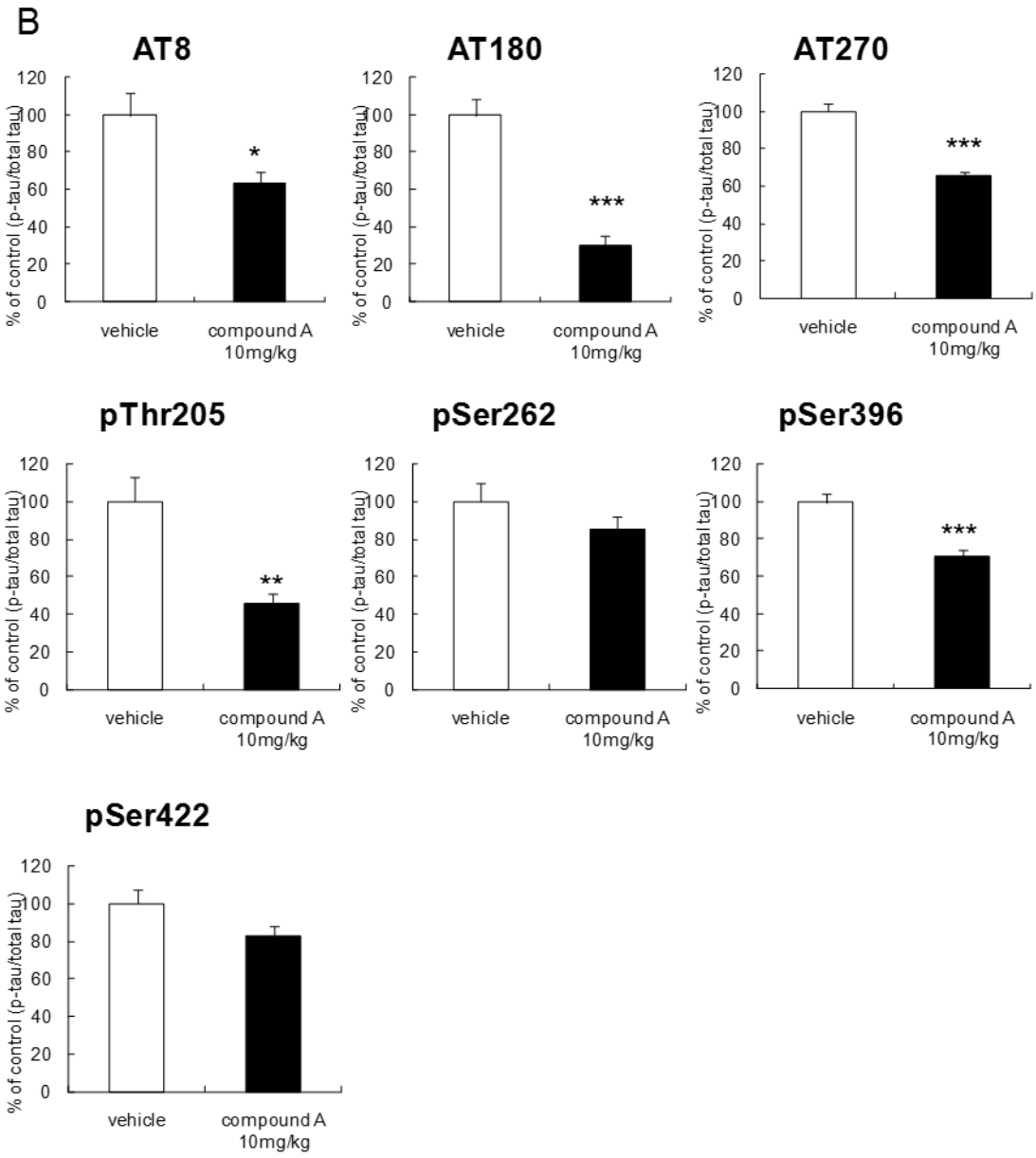
B
AT8
AT180
AT270
pThr205
pSer262
pSer396
pSer422
% of control (p-tau/total tau)
0
20
40
60
80
100
120
*
**
***
vehicle
compound A
10mg/kg

C

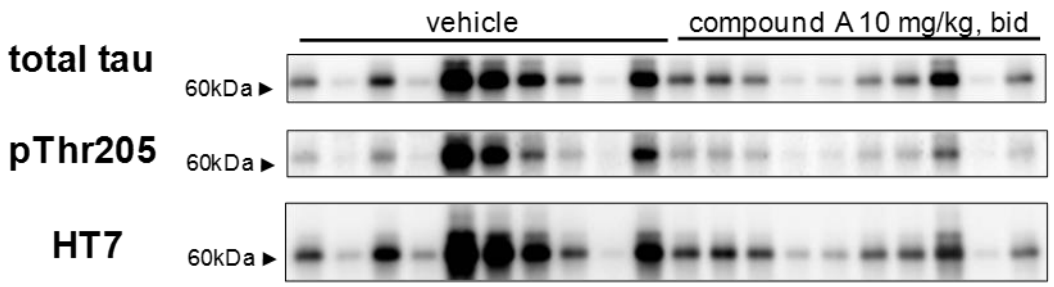
vehicle
compound A 10 mg/kg, bid
total tau
60kDa ►
pThr205
60kDa ►
HT7
60kDa ►

D

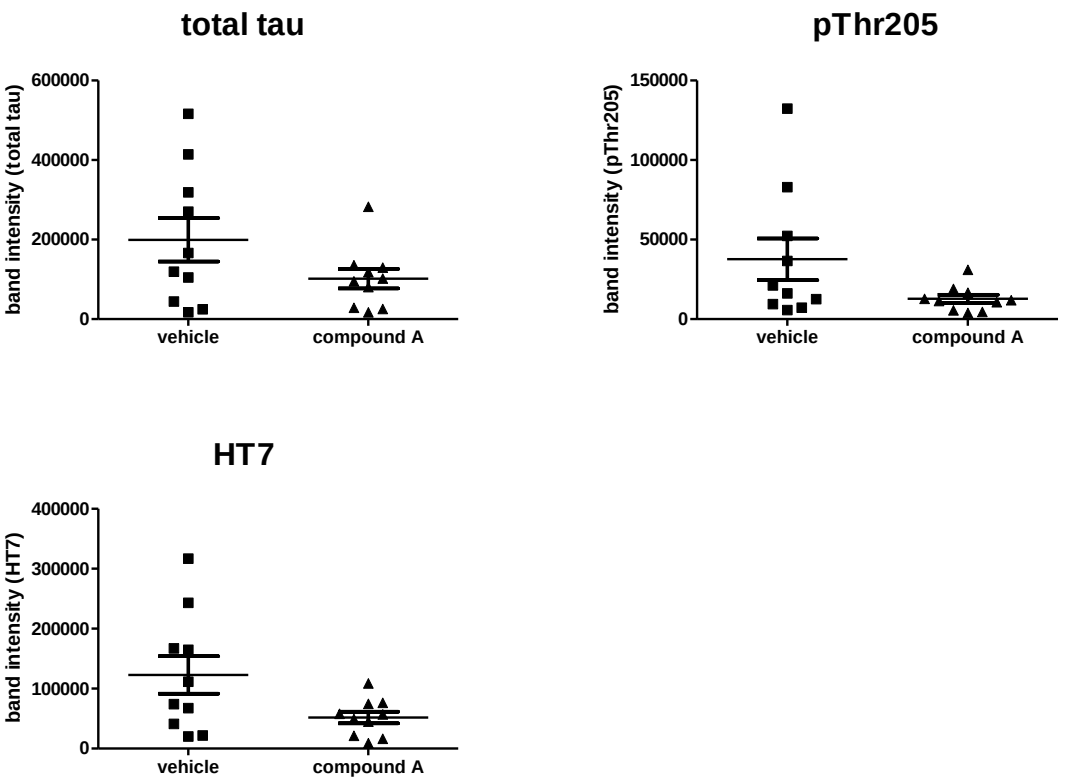
total tau
band intensity (total tau)
600000
400000
200000
0
vehicle
compound A
pThr205
band intensity (pThr205)
150000
100000
50000
0
vehicle
compound A
HT7
band intensity (HT7)
400000
300000
200000
100000
0
vehicle
compound A

Figure 10. Immunohistochemical analysis of compound **A** treated JNPL3 mice brains. Compound **A** was administered at a dose of 10 mg/kg twice daily by oral gavage for 1 month to female JNPL3 mice (5.5 months old). PThr205 and HT7 immunostaining were performed in vehicle treated mice (pThr205; *A-D*, HT7; *I-L*) and compound **A** treated mice (pThr205; *E-H*, HT7; *M-P*), in the hippocampus (A, E, I, M) (magnification, 40x), the CA1 (B, F, J, N) (magnification, 600x), the CA3 (C, G, K, O) (magnification, 600x), or the dentate gyrus regions (D, H, L, P) (magnification, 600x). Hematoxylin was used for counterstaining.

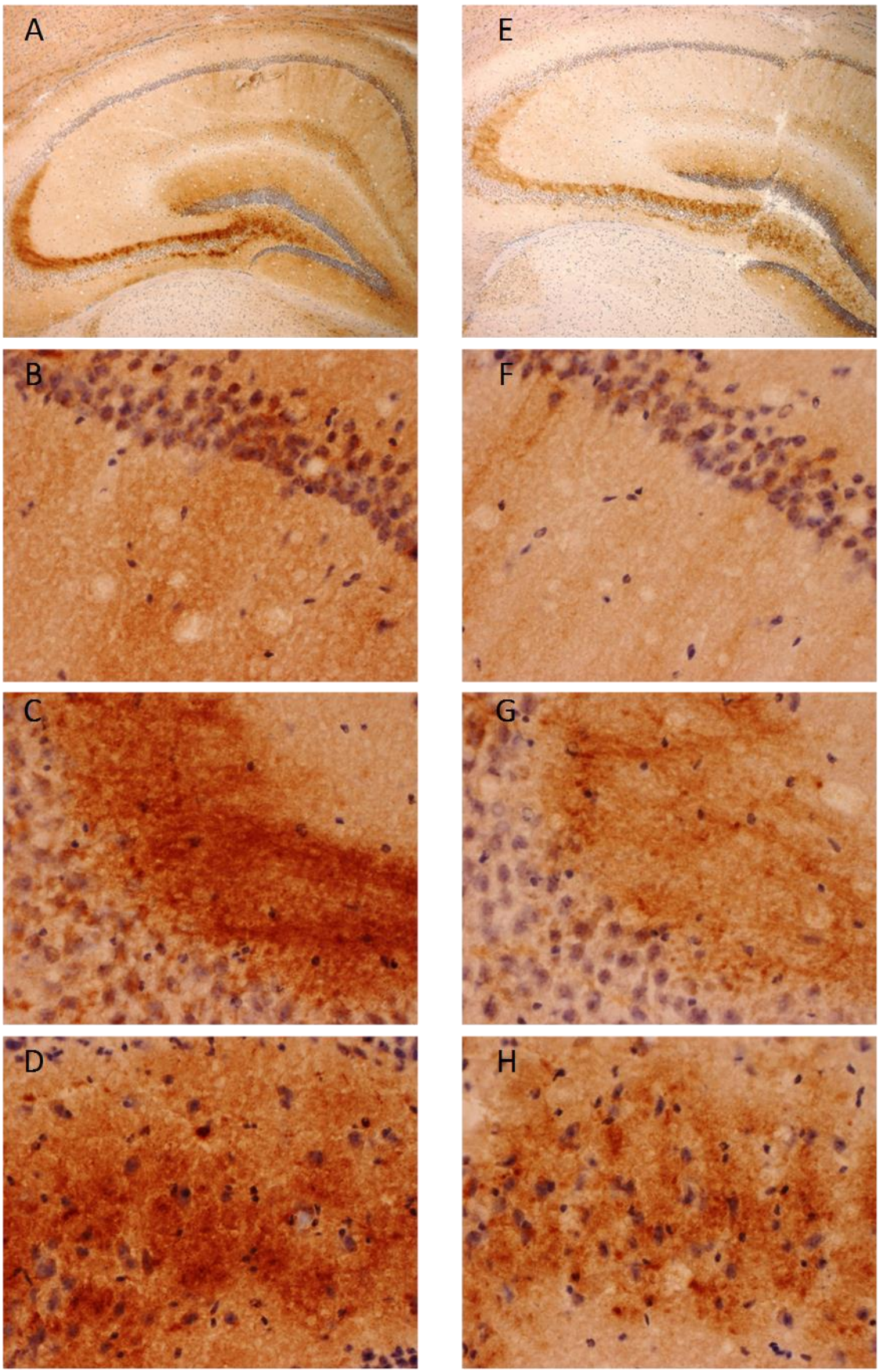
A
E
B
F
C
G
D
H

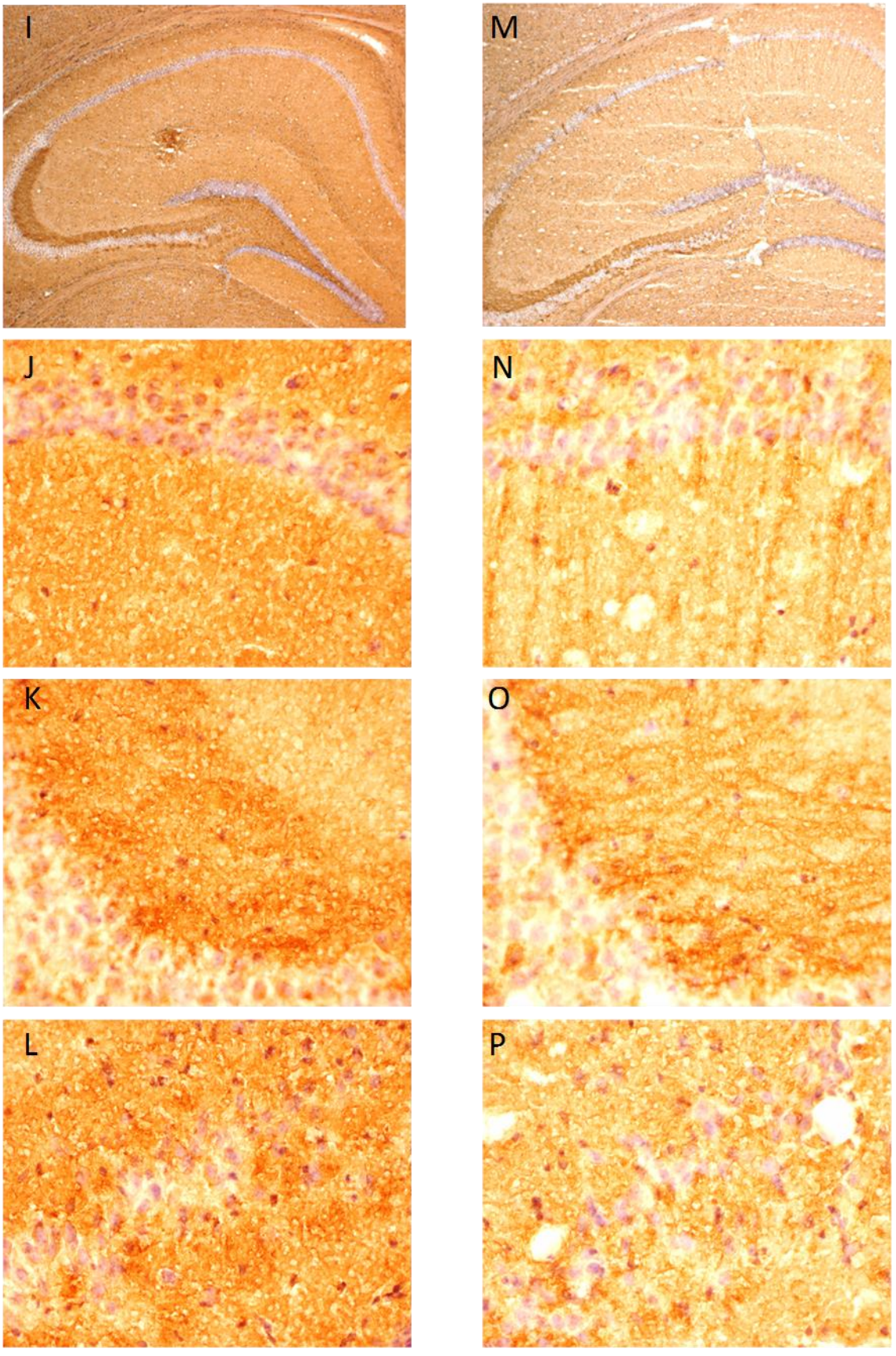
I
M
J
N
K
O
L
P

Figure 11. Immunohistochemical analysis of compound **A** treated JNPL3 mice brains. Compound **A** was administered at a dose of 26 mg/kg/day by feeding for 1 month to male JNPL3 mice (12.5 months old). PThr205 and HT7 immunostaining were performed in vehicle treated mice (pThr205; *A-D*, HT7; *I-L*) and compound **A** treated mice (pThr205; *E-H*, HT7; *M-P*), in the hippocampus (*A, E, I, M*) (magnification, 40x), the CA1 (*B, F, J, N*) (magnification, 600x), the CA3 (*C, G, K, O*) (magnification, 600x), or the dentate gyrus regions (*D, H, L, P*) (magnification, 600x). Hematoxylin was used for counterstaining.

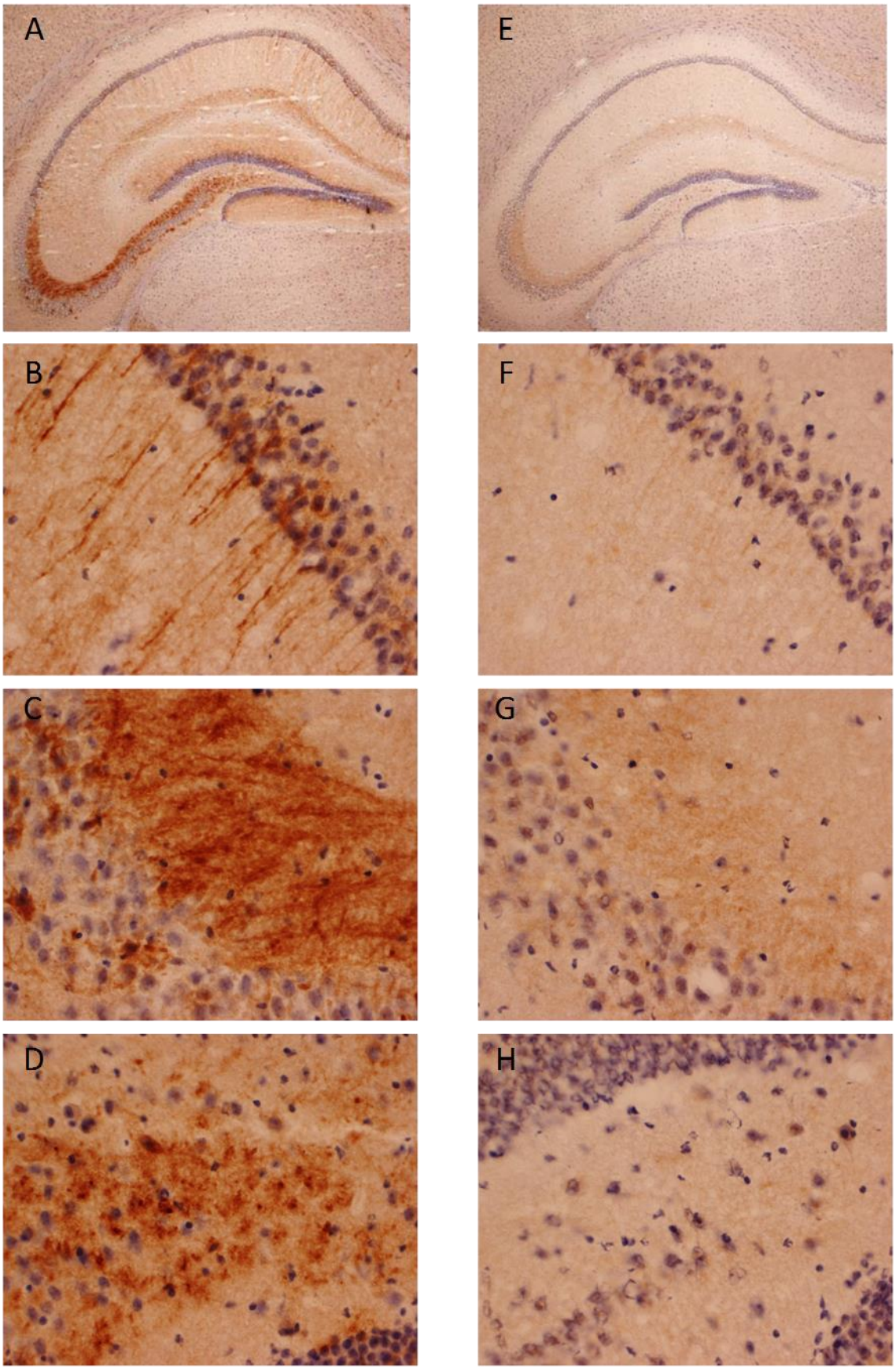
A
E
B
F
C
G
D
H

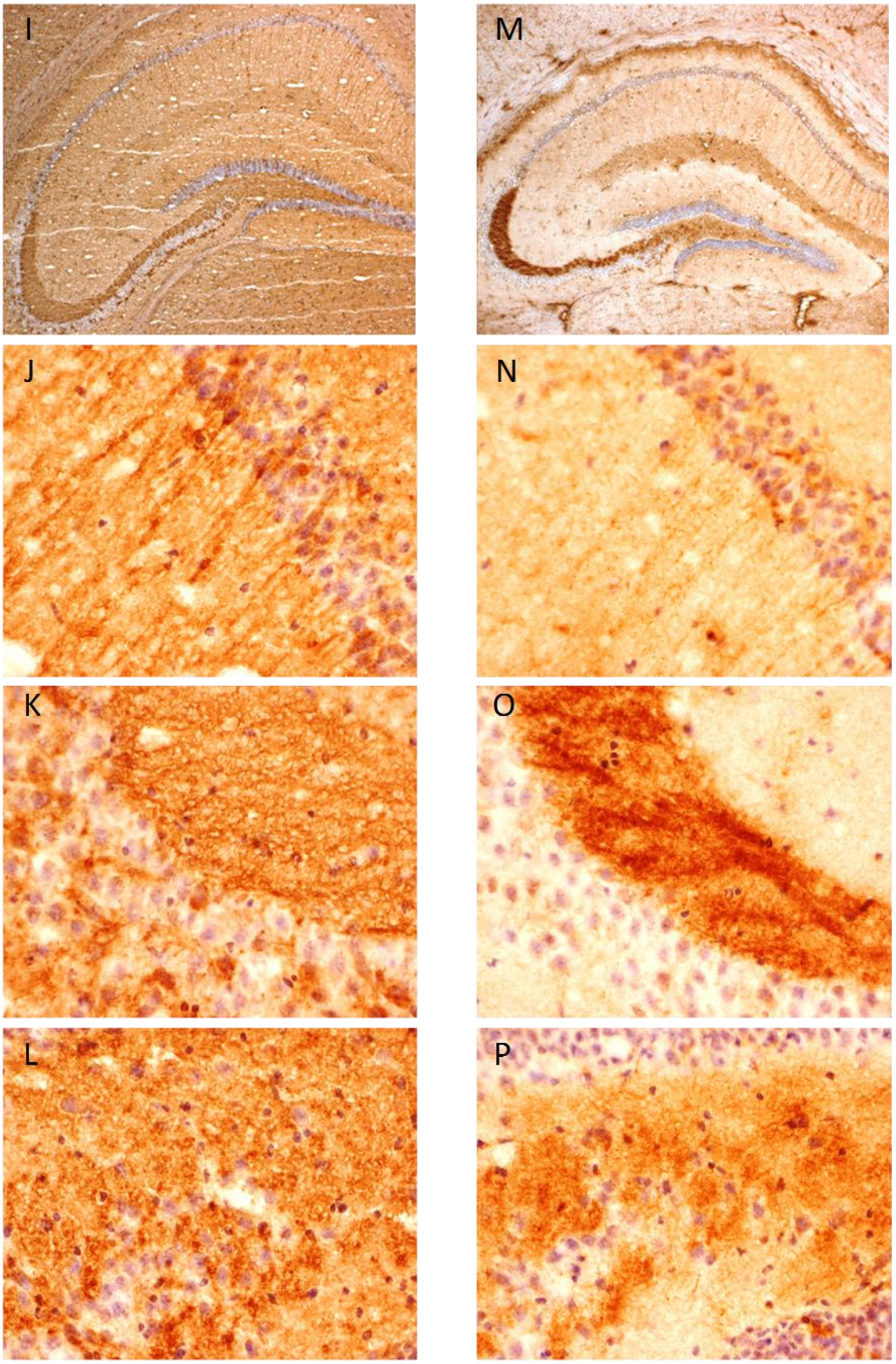
I
M
J
N
K
O
L
P

Figure 12. Effects of compound **A** on insoluble/aggregated tau in JNPL3 mouse brain. Male JNPL3 mice, age 12.5 months, were treated by feeding with chow containing 200 mg compound **A** per kg chow (0.02%) for 1 month. In this dosing paradigm, 26 mg/kg/day of compound **A** were administered to mice. *A*, Proteins from sarkosyl insoluble fractions were separated by SDS-PAGE and detected by total tau, pThr205, and HT7 antibodies. The sarkosyl insoluble fraction of an AD patient hippocampus sample (AD) was run in parallel. *B*, Immunoblot bands were quantified by densitometry. Data represent means ± S.E.M. of 9 or 10 animals. Significance is defined as * $p \leq 0.05$ (*t*-test) in comparison to the vehicle administered group.

A

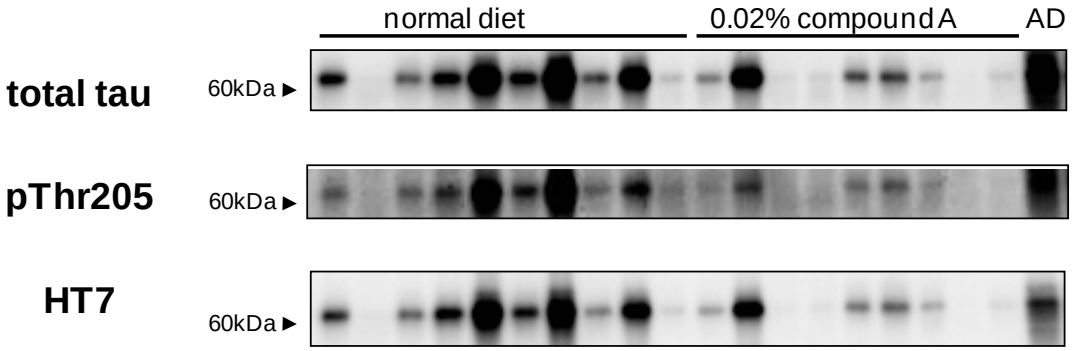
normal diet
0.02% compound A
AD
total tau
60kDa ►
pThr205
60kDa ►
HT7
60kDa ►

B

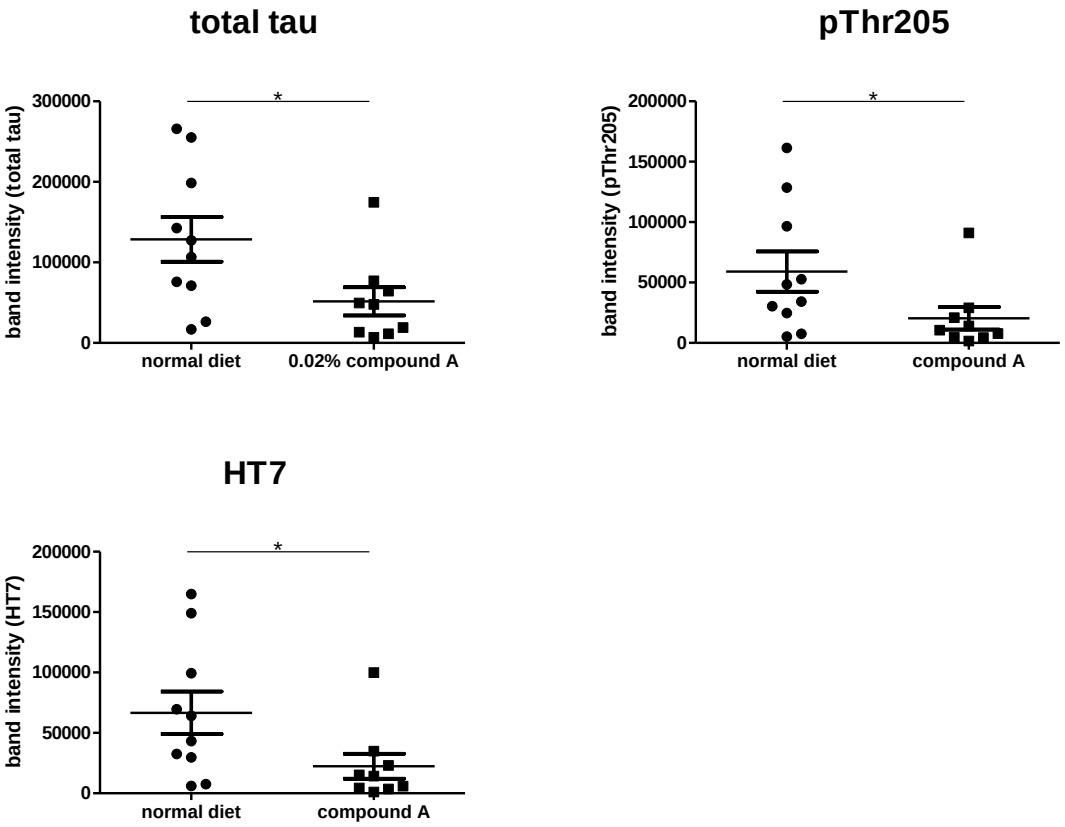
total tau
band intensity (total tau)
300000
200000
100000
0
*
normal diet
0.02% compound A
pThr205
band intensity (pThr205)
200000
150000
100000
50000
0
*
normal diet
compound A
HT7
band intensity (HT7)
200000
150000
100000
50000
0
*
normal diet
compound A

Supplemental Figure 2. Effects of compound A on food intake and body weight of JNPL3 mouse. Male JNPL3 mice, age 12.5 months, were treated by feeding with chow containing 200 mg compound A per kg chow (0.02%) for 1 month.

Body weight

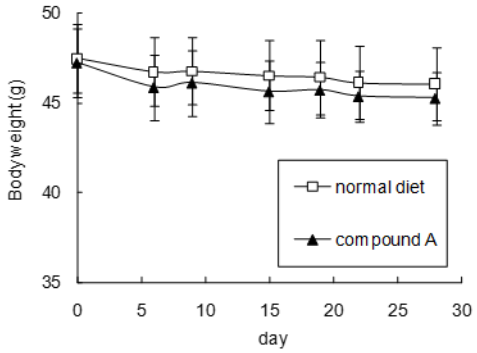

Food intakes

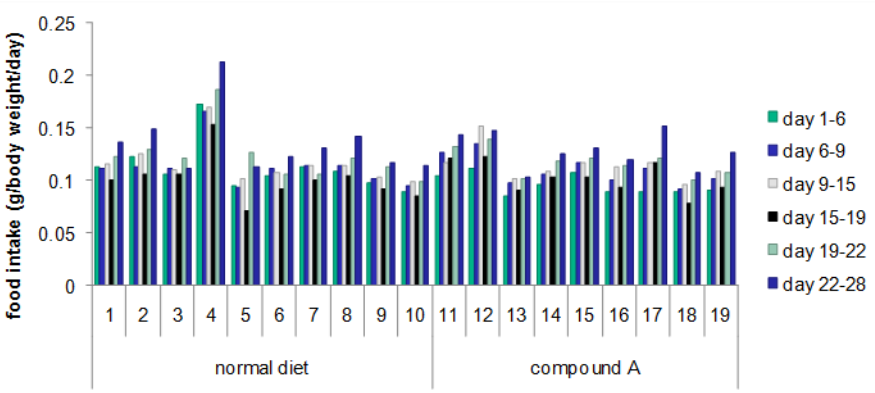

Supplemental Figure 3. Effects of compound **A** on insoluble/aggregated tau in JNPL3 mouse brain. Male JNPL3 mice, age 12.5 months, were treated by feeding with chow containing 200 mg compound **A** per kg chow (0.02%) for 1 month. In this dosing paradigm, 26 mg/kg/day of compound **A** were administered to mice. A, Proteins were extracted by RAB-RIPA-Formic acid (FA) extraction procedure. Each fraction was separated by SDS-PAGE and detected by total tau and pThr205 antibodies. B, Immunoblot bands were quantified by densitometry. Data represent means ± S.E.M. of 9 or 10 animals. Significance is defined as * $p \leq 0.05$ and *** $p \leq 0.001$ (*t*-test) in comparison to the vehicle administered group.

A

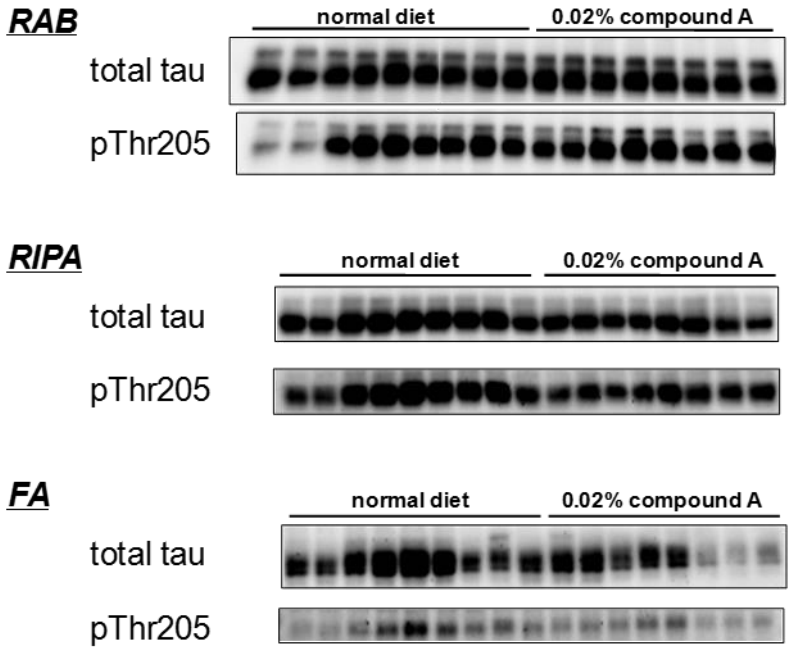
RAB
normal diet
0.02% compound A
total tau
pThr205
RIPA
normal diet
0.02% compound A
total tau
pThr205
FA
normal diet
0.02% compound A
total tau
pThr205

B

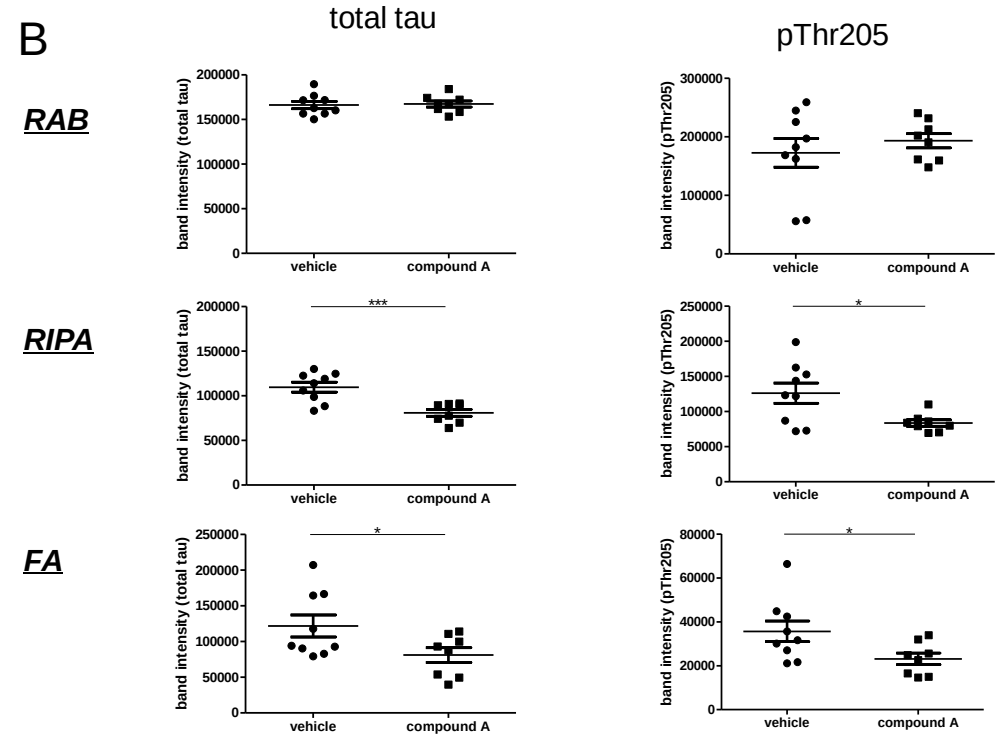
total tau
pThr205
RAB
band intensity (total tau)
band intensity (pThr205)
vehicle
compound A
RIPA
***
*
FA
*
*

General discussion

In this study, I studied the potential of tau targeting strategies for AD treatment. There are various mechanisms related to tau toxicity, such as gene/protein expression, phosphorylation, degradation, and aggregation. Among these, I have focused on gene expression and phosphorylation, and studied details of tau gene expression modulation through transcription factor Sp1 and tau phosphorylation reduction by a tau kinase inhibitor.

In the chapter 1, I investigated modulation of tau gene expression. Though tau has an important role in microtubule assembly and microtubule stability for maintaining normal axonal integrity and neuronal function, loss of tau would not show any gross physical or behavioral abnormalities in the light of evidence from tau knockout mice study (4). In addition, some basic research indicated that reduction of tau expression is expected to exert efficacy of AD treatment. It was reported that Aβ induced toxicity was reduced in primary cultured neurons from tau knockout mice. Premature mortality and memory deficits in APP transgenic mice were prevented by crossing with tau knockout mice (4). Taken together, reduction of tau gene expression is an attractive strategy for AD treatment.

I investigated DNA recognition mode of Sp1 zinc finger motif in detail to obtain basic knowledge for tau expression modulation via Sp1. From the analysis, I found that the C-terminal finger induced conformation change in DNA structure of the N-terminal finger binding regions, and that the conformation change affected DNA recognition mode of the N-terminal finger. Sp1 have various substrates arise from the flexible base recognition mode of N-terminal finger. Unique amino acid sequence of N-terminal finger in "recognition helix" comparing to other C2H2 type zinc fingers has been considered to be one of the reasons for the flexible base recognition mode (93). From my research results, conformation change in DNA structure of the N-terminal finger would also contribute to the flexible base recognition mode of Sp1 zinc finger motif.

In addition to the pivotal role in tau gene expression regulation, recent growing number of evidences suggested the crucial roles of Sp1 in AD pathogenesis. In a pathway enrichment analysis on genome-wide association data from 742 Alzheimer's Disease Neuroimaging Initiative (ADNI) participants, Sp1 was revealed as a master regulator gene of multiple known AD-risk genes (94). Also, from the large-scale gene expression analysis related to aging, it is reported that Sp1 plays an important role in aging, which is the most common risk factor of AD (95). So targeting Sp1 is one of the attractive strategies for AD treatment development. It was reported that treatment of tolfenamic acid and mithramycin A, Sp1 inhibitors, ameliorated tau pathology, Aβ pathology, and cognitive impairment in AD model mice (96-98). As Sp1 interact with many genes, Sp1 can not only affect a number of AD related genes (e.g. APP, ApoE, BACE1, MAPT) but also many other genes related to transcription, tumor suppression and DNA repair (99). Consequently, Sp1 targeting approach has concerns of side effects as well as potential of efficacy. One of the possible solutions to avoid the side effects is 'Sp1 modulator', which can only affect the expression of essential genes for beneficial effects. There are no reports describing Sp1 and AD target gene(s) selective inhibitors so far, but YM155 would be a nice reference compound. It was reported that YM155 could selectively inhibit Sp1-survivin gene expression without inhibiting other Sp1 controlled gene promotors (e.g. p21, thymidine kinase) (100). In addition, as it was suggested that Sp1 has an important role in tau (MAPT) promoter's neuronal expression with undetermined cofactor(s) (8), cofactor(s) information might be a clue to find Sp1-tau (MAPT) selective inhibitors. To raise the possibility of success to obtain Sp1 modulator compounds for AD treatment, it is necessary to deeply understand the structural and biochemical information of Sp1-target gene interaction. My finding would be helpful for understanding basis for Sp1-target gene interaction, and also designing tau expression modulators via Sp1.

In the second chapter, I studied about tau phosphorylation reduction by GSK-3 inhibitor. The precise mechanism of tau toxicity remains unclear so far, tau phosphorylation has been considered to be a pivotal step of tau toxicity. GSK-3β is a main tau kinase and responsible for most sites of tau phosphorylation (101). Although compound A has inhibitory activity against CDK2/CycA with 10^{-7}M order IC_{50} value, the influence of CDK2/CycA inhibition could be negligible owing to little contribution of CDK2/CycA in tau phosphorylation (101) and no CDK2/CycA expression in brain (102). Therefore, compound A, a potent and selective GSK-3 inhibitor, is an ideal tool to investigate potential of tau phosphorylation reduction thorough GSK-3 inhibition for AD treatment. From my study, it is indicated that tau phosphorylation reduction thorough GSK-3 inhibition would be effective even in the later stage of pathology. This is significant finding for development of tau-targeting AD treatment.

My research suggests the potential of compound A for AD treatment, but it needs to be confirmed whether compound A could have efficacy on cognitive deficit. Since a previous report has already indicated the efficacy of ATP-competitive GSK-3 inhibitor on cognitive deficit in preclinical studies (103), it is expected that compound A also have efficacy on cognitive deficit. Moreover, it is indispensable to discuss about concerns of side effects related to GSK-3 inhibition. GSK-3 plays crucial roles in various physiological processes via its substrates, such as metabolism, development, and differentiation (104). Especially, β-catenin, one of GSK-3 substrates, is famous for its role in tumorgenesis and tumor progression (105). Most of reported GSK-3 inhibitors, including compound A, are ATP-competitive inhibitors, and it is theoretically impossible to have substrates selectivity for ATP-competitive kinase inhibitors. To avoid severe side effects, development of novel type of GSK-3 inhibitors, such as "substrate-competitive inhibitors" and "modulators", would be a great challenge for the future of AD treatment.

Global multi-center neuroimaging study result indicated that pathology precede clinical symptom in AD (2). Currently, people pay much attention to tau targeting strategy in response to several disappointing clinical results of Aβ targeting drugs. Much later intervention can be acceptable for tau targeting strategy than Aβ targeting strategy considering disease course and pathology establishment (106, 107). Indeed, in my study, tau targeting strategy would be effective in the later stage of pathology. In addition to the above mentioned approach, recent research progress in the tau-targeting strategy, such as anti-tau antibodies and tau antisense oligonucleotides, is remarkable (108, 109). It is expected that effective AD therapy will be developed in near future from tau targeting strategy.

Acknowledgements

I am most grateful to Professors Osamu Numata and Tomoki Chiba, and Associate Professors Kentaro Nakano and Ryusuke Niwa, University of Tsukuba, for their continuous guidance and valuable discussions through my doctoral program.

I thank H. Nagaya, T. Wada, and M. Miyamoto for their encouragement and helpful advice. I am also grateful to T. Onishi, S. Watanabe, T. Hioki, H. Miya, K. Kakoi, S. Yao, S. Itono, H. Fujita, M. Yamaguchi, K. Yamamoto and M. Takizawa for helpful discussions.

Finally, I would like to appreciate my family for supporting my life in University of Tsukuba.

References

1. Wimo A., Guerchet M., Ali G. C., Wu Y. T., Prina A. M., Winblad B., Jönsson L., Liu Z., and Prince M. (2017) The worldwide costs of dementia 2015 and comparisons with 2010. Alzheimers Dement, 13, 1-7.
2. Weiner M. W., Veitch D. P., Aisen P. S., Beckett L. A., Cairns N. J., Green R. C., Harvey D., Jack C. R., Jagust W., Liu E., Morris J. C., Petersen R. C., Saykin A. J., Schmidt M. E., Shaw L., Siuciak J. A., Soares H., Toga A. W., Trojanowski J. Q.; Alzheimer's Disease Neuroimaging Initiative (2012) The Alzheimer's disease neuroimaging initiative: a review of papers published since its inception. Alzheimers Dement, 1 Suppl, S1-S68.
3. Ossenkoppele R., Schonhaut D. R., Schöll M., Lockhart S. N., Ayakta N., Baker S. L., O'Neil J. P., Janabi M., Lazaris A., Cantwell A., Vogel J., Santos M., Miller Z. A., Bettcher B. M., Vossel K. A., Kramer J. H., Gorno-Tempini M. L., Miller B. L., Jagust W. J., and Rabinovici G. D. (2016) Tau PET patterns mirror clinical and neuroanatomical variability in Alzheimer's disease. Brain, 139, 1551-1567.
4. Ke Y. D., Suchowerska A. K., van der Hoven J., De Silva D. M., Wu C. W., van Eersel J., Ittner A., and Ittner L. M. (2012) Lessons from tau-deficient mice. Int J Alzheimers Dis, 2012, 873270
5. Šimić G., Babić Leko M., Wray S., Harrington C., Delalle I., Jovanov-Milošević N., Bažadona D., Buée L., de Silva R., Di Giovanni G., Wischik C., Hof P. R. (2016) Tau Protein Hyperphosphorylation and Aggregation in Alzheimer's Disease and Other Tauopathies, and Possible Neuroprotective Strategies. Biomolecule, 6, 6.
6. Li C. and Götz J., (2017) Tau-based therapies in neurodegeneration: opportunities and challenges. Nat Rev Drug Discov, 2017, Oct 6.
7. Iqbal K., Liu F., and Gong C. X. (2016) Tau and neurodegenerative disease: the story so far. Nat Rev Neurol, 12, 15-27.

8. Heicklen-Klein A., and Ginzburg I. (2000) Tau promoter confers neuronal specificity and binds Sp1 and AP-2. J Neurochem, 75, 1408-1418.
9. Santpere G., Nieto M., Puig B., and Ferrer I. (2006) Abnormal Sp1 transcription factor expression in Alzheimer disease and tauopathies. Neurosci Lett, 397, 30-34.
10. Wolfe S. A., Nekludova L., and Pabo C. O. (1999) DNA recognition by Cys2His2 zinc finger proteins. Annu Rev Biophys Biomol Struct, 29, 183−212.
11. Dervan P. B. and Bürli R. W. (1999) Sequence-specific DNA recognition by polyamides. Curr Opin Chem Biol, 3, 688−693.
12. Pavletich N. P. and Pabo C. O. (1991) Zinc finger-DNA recognition: crystal structure of a Zif268-DNA complex at 2.1 A . Science, 252, 809−817.
13. Elrod-Erickson M., Rould M. A., Nekludova L., and Pabo C. O. (1996) Zif268 protein-DNA complex refined at 1.6 A: a model system for understanding zinc finger-DNA interactions. Structure, 4, 1171−1180.
14. Choo Y. (1998) End effects in DNA recognition by zinc finger arrays. Nucleic Acids Res, 26, 554−557.
15. Zang W.-Q., Veldhoe N., and Romaniuk P. J. (1995) Effects of zinc finger mutations on the nucleic acid binding activities of Xenopus transcription factor IIIA. Biochemistry, 34, 15545−15552.
16. Nakagama H., Heinrich G., Pelletier J., and Housman D. E. (1995) Sequence and structural requirements for high-affinity DNA binding by the WT1 gene product. Mol Cell Biol, 15, 1489−1498.
17. Desjarlais J. R. and Berg J. M. (1993) Use of a zinc-finger consensus sequence framework and specificity rules to design specific DNA binding proteins. Proc Natl Acad Sci USA, 90, 2256−2260.

18. Wolfe S. A., Greisman H. A., Ramm E. I., and Pabo C. O. (1999) Analysis of zinc fingers optimized via phage display: evaluating the utility of a recognition code. J Mol Biol, 285, 1917−1934.
19. Dynan W. S. and Tjian R. (1983) Isolation of transcription factors that discriminate between different promoters recognized by RNA polymerase II. Cell, 32, 669−680.
20. Kadonaga J. T., Carne, K. R., Masiarz F. R., and Tjian R. (1987) Isolation of cDNA encoding transcription factor Sp1 and functional analysis of the DNA binding domain. Cell, 51, 1079−1090.
21. Kadonaga J. T., Jones K. A., and Tjian R. (1986) Promoter-specific activation of RNA polymerase II transcription by Sp1. Trends Biochem Sci, 11, 20−23.
22. Bucher P. (1990) Weight matrix descriptions of four eukaryotic RNA polymerase II promoter elements derived from 502 unrelated promoter sequences. J Mol Biol, 212, 563−578.
23. Miller J., McLachlan A. D., and Klug A. (1985) Repetitive zinc-binding domains in the protein transcription factor IIIA from Xenopus oocytes. EMBO J, 4, 1609−1614.
24. Brown R. S., Sander C., and Argos P. (1985) The primary structure of transcription factor TFIIIA has 12 consecutive repeats. FEBS Lett, 186, 271−274.
25. Kriwacki R. W., Schultz S. C. Steitz T. A., and Caradonna J. P. (1992) Sequence-specific recognition of DNA by zinc-finger peptides derived from the transcription factor Sp1. Proc Natl Acad Sci USA, 89, 9759−9763.
26. Berg J. M. (1992) Sp1 and the subfamily of zinc finger proteins with guanine-rich binding sites. Proc Natl Acad Sci USA, 89, 11109−11110.

27. Kuwahara J., Yonezawa A., Futamura M., and Sugiura Y. (1993) Binding of transcription factor Sp1 to GC box DNA revealed by footprinting analysis: Different contact of three zinc fingers and sequence recognition mode. Biochemistry, 32, 5994−6001.
28. Yokono M., Saegusa N., Matsushita K., and Sugiura Y. (1998) Unique DNA binding mode of the N-terminal zinc finger of transcription factor Sp1. Biochemistry, 37, 6824−6832.
29. Nagaoka M. and Sugiura Y. (1996) Distinct phosphate backbone contacts revealed by some mutant peptides of zinc finger protein Sp1: Effect of protein-induced bending on DNA recognition. Biochemistry, 35, 8761−8768.
30. Brenowitz M., Senear D. F., Shea M. A., and Ackes G. K. (1986) Quantitative DNase footprint titration: a method for studying protein-DNA interactions. Methods Enzymol, 130, 132−181.
31. Kuwahara J. and Coleman J. E. (1990) Binding of transcription factor Sp1 to GC box DNA revealed by footprinting analysis: Different contact of three zinc fingers and sequence recognition mode. Biochemistry, 29, 8627−8631.
32. Frankel A. D., Berg J. M., and Pabo C. O. (1987) Metal-dependent folding of a single zinc finger from transcription factor IIIA. Proc Natl Acad Sci USA, 84, 4841−4845.
33. Hori Y., Suzuk K., Okuno Y., Nagaok, M., Futaki S., and Sugiura Y. (2000) Artificial zinc finger peptide containing a novel His4 domain. J Am Chem Soc, 122, 7648−7653.
34. Laity J. H., Dyson J., and Wright P. E. (2000) DNA-induced α-helix capping in conserved linker sequences is a determinant of binding affinity in Cys2-His2 zinc fingers. J Mol Biol, 295, 719−727.
35. Matsushita K. and Sugiura Y. (2001) Effect of arginine mutation of alanine-556 on DNA recognition of zinc finger protein Sp1. Bioorg Med Chem, 9, 2259-2267.

36. Pavletich N. P and Pabo C. O. (1993) Crystal structure of a five-finger GLI-DNA complex: new perspectives on zinc fingers. Science, 261, 1701−1707.
37. Fairall L., Schwabe J. W. R., Chapman L., Finch J. T., and Rhodes D. (1993) The crystal structure of a two zinc-finger peptide reveals an extension to the rules for zinc-finger/DNA recognition. Nature, 366, 483−487.
38. Houbaviy H. B., Usheva A., Shenk T., and Burle S. K. (1996) Cocrystal structure of YY1 bound to the adeno-associated virus P5 initiator. Proc Natl Acad Sci USA, 93, 13577−13582.
39. Nolte R. T., Conlin R. M., Harrison S. C., and Brown R. S. (1998) Differing roles for zinc fingers in DNA recognition: structure of a six-finger transcription factor IIIA complex. Proc Natl Acad Sci USA, 95, 2938−2943.
40. Sjφttem E., Andersen C., and Johansen T. (1997) Structural and functional analyses of DNA bending induced by Sp1 family transcription factors. J Mol Biol, 267, 490−504.
41. Shi Y. and Berg J. M. (1996) DNA unwinding induced by zinc finger protein binding. Biochemistry, 35, 3845−3848.
42. Suck D., Lahm A., and Oefner C. (1988) Structure refined to 2 Å of a nicked DNA octanucleotide complex with DNase. Nature, 332, 464−468.
43. Nagaoka M., Kaji T., Imanishi M., Hori Y., Nomura W., and Sugiura Y. (2001) Multiconnection of identical zinc finger: implication for DNA binding affinity and unit modulation of the three zinc finger domain. Biochemistry, 40, 2932-2941.
44. Reber E. J. and Pabo C. O. (1994) Zinc finger phage: affinity selection of fingers with new DNA-binding specificities. Science, 263, 671−673.
45. Choo Y., and Klug A. (1994) Toward a code for the interactions of zinc fingers with DNA: selection of randomized fingers displayed on phage. Proc Natl Acad Sci USA, 91, 11163−11167.

46. Choo Y., and Klug A. (1994) Selection of DNA binding sites for zinc fingers using rationally randomized DNA reveals coded interactions. Proc Natl Acad Sci USA, 91, 11168−11172.
47. Jamieson A. C., Kim S. H., and Wells J. A. (1994) In vitro selection of zinc fingers with altered DNA-binding specificity. Biochemistry, 33, 5689−5695.
48. Dickson D. W. (1997) Neurodegenerative diseases with cytoskeletal pathology: a biochemical classification. Ann Neurol, 42, 541-544.
49. Lee V. M., Goedert M., and Trojanowski J. Q. (2001) Neurodegenerative tauopathies. Annu Rev Neurosci, 24, 1121-1159.
50. Braak H., and Braak E. (1991) Neuropathological staging of Alzheimer-related changes. Acta Neuropathology, 82, 239-259.
51. Braak H., and Braak E. (1991) Demonstration of amyloid deposits and neurofibrillary changes in whole brain sections. Brain Pathology, 1, 213-216.
52. Ballatore C, Lee V. M., and Trojanowski J. Q. (2007) Tau-mediated neurodegeneration in Alzheimer's disease and related disorders. Nat Rev Neurosci, 8, 663-672.
53. Alonso A. C., Zaidi T., Grundke-Iqbal I., and Iqbal K. (1994) Role of abnormally phosphorylated tau in the breakdown of microtubules in Alzheimer disease. Proc Natl Acad Sci USA, 91, 5562-5566.
54. Alonso A. C., Grundke-Iqbal I., and Iqbal K. (1996) Alzheimer's disease hyperphosphorylated tau sequesters normal tau into tangles of filaments and disassembles microtubules. Nat Med, 2, 783-787.
55. Wang J. Z., Grundke-Iqbal I., and Iqbal K. (1996) Restoration of biological activity of Alzheimer abnormally phosphorylated tau by dephosphorylation with protein phosphatase-2A, -2B and -1. Brain Res Mol Brain Res, 38, 200-208.

56. Mandelkow E. M., Stamer K., Vogel R., Thies E., and Mandelkow E. (2003) Clogging of axons by tau, inhibition of axonal traffic and starvation of synapses. Neurobiol Aging, 8, 1079-1085.

57. Santacruz K., Lewis J., Spires T., Paulson J., Kotilinek L., Ingelsson M., Guimaraes A., DeTure M., Ramsden M., McGowan E., Forster C., Yue M., Orne J., Janus C., Mariash A., Kuskowski M., Hyman B., Hutton M., and Ashe K. H., (2005) Tau suppression in a neurodegenerative mouse model improves memory function. Science, 309, 476-481.

58. Yoshiyama Y., Higuchi M., Zhang B., Huang S. M., Iwata N., Saido T. C., Maeda J., Suhara T., Trojanowski J. Q., and Lee V. M., (2007) Synapse loss and microglial activation precede tangles in a P301S tauopathy mouse model. Neuron, 53, 337-351.

59. Drewes G., Lichtenberg-Kraag B., Doring F., Mandelkow E. M., Biernat J., Goris J., Doree M., and Mandelkow E. (1992) Mitogen activated protein (MAP) kinase transforms tau protein into an Alzheimer-like state. EMBO J, 6, 2131-2138.

60. Ishiguro K., Takamatsu M., Tomizawa K., Omori A., Takahashi M., Arioka M., Uchida T., and Imahori K. (1992) Tau protein kinase I converts normal tau protein into A68-like component of paired helical filaments. J Biol Chem, 267, 10897-10901.

61. Ledesma M. D., Correas I., Avila J., and Diaz-Nido J. (1992) Implication of brain cdc2 and MAP2 kinases in the phosphorylation of tau protein in Alzheimer's disease. FEBS Lett, 308, 218-224.

62. Morishima-Kawashima, M., Hasegawa M., Takio K., Suzuki M., Yoshida H., Titani K., and Ihara Y. (1995) Proline-directed and non-proline-directed phosphorylation of PHF-tau. J Biol Chem 270, 823-829.

63. Pei J.-J., Grundke-Iqbal I., Iqbal K., Bogdanovic N., Winblad B., and Cowburn R. F. (1998) Accumulation of cyclin-dependent kinase 5 (cdk5) in neurons with early stages of Alzheimer's disease neurofibrillary degeneration. Brain Res, 797, 267-277.

64. Sengupta A., Wu Q., Grundke-Iqbal I., Iqbal K., and Singh T. J. (1997) Potentiation of GSK-3-catalyzed Alzheimer-like phosphorylation of human tau by cdk5. Mol Cell Biochem, 167, 99-105.

65. Flaherty, D. B., Soria, J. P., Tomasiewicz, H. G., and Wood, J.G. (2000) Phosphorylation of human tau protein by microtubule-associated kinases: GSK3beta and cdk5 are key participants. J Neurosci Res, 62, 463-472.

66. Wagner U., Utton M., Gallo J. M., and Miller C. C. (1996) Cellular phosphorylation of tau by GSK-3 beta influences tau binding to microtubules and microtubule organization. J Cell Sci, 109, 1537-43.

67. Lucas J. J., Hernandez F., Gomez-Ramos P., Moran M. A., Hen R., and Avila J. (2001). Decreased nuclear beta-catenin, tau hyperphosphorylation and neurodegeneration in GSK-3beta conditional transgenic mice. EMBO J, 20, 27-39.

68. Hernandez F., Borrell J., Guaza C., Avila J., and Lucas J. J. (2002) Spatial learning deficit in transgenic mice that conditionally over-express GSK-3beta in the brain but do not form tau filaments. J. Neurochem, 83, 1529-1533.

69. Pei J.-J., Tanaka T., Tung Y.-C., Braak E., Iqbal K., and Grundke-Iqbal I. (1997) Distribution, levels, and activity of glycogen synthase kinase-3 in the Alzheimer disease brain. J Neuropathol Exp Neurol, 56, 70-78.

70. Pei J.-J., Braak E., Braak H., Grundke-Iqbal I., Iqbal,K., Winblad B., and Cowburn R. F. (1999) Distribution of active glycogen synthase kinase 3beta (GSK-3beta) in brains staged for Alzheimer disease neurofibrillary changes. J Neuropathol Exp Neurol, 58, 1010-1019.

71. Cohen P., and Goedert M. (2004) GSK3 inhibitors: development and therapeutic potential. Nat Rev Drug Discov, 3, 479-489.

72. Meijer L., Flajolet M., and Greengard P. (2004) Pharmacological inhibitors of glycogen synthase kinase 3. Trends Pharmacol Sci, 9, 471-480.

73. Churcher I. (2006) Tau therapeutic strategies for the treatment of Alzheimer's disease. Curr Top Med Chem, 6, 579-595.

74. Mazanetz M. P., and Fischer, P. M. (2007) Untangling tau hyperphosphorylation in drug design for neurodegenerative diseases. Nat Rev Drug Discov, 6, 464-479.

75. Noble W., Planel E., Zehr C., Olm V., Meyerson J., Suleman F., Gaynor K., Wang L., LaFrancois J., Feinstein B., Burns M., Krishnamurthy P., Wen Y., Bhat R., Lewis J., Dickson D., and Duff K. (2005) Inhibition of glycogen synthase kinase-3 by lithium correlates with reduced tauopathy and degeneration in vivo. Proc Natl Acad Sci USA, 102, 6990-6995.

76. Selenica M. L., Jensen H. S., Larsen A. K., Pedersen M. L., Helboe L., Leist M., and Lotharius J. (2007) Efficacy of small-molecule glycogen synthase kinase-3 inhibitors in the postnatal rat model of tau hyperphosphorylation. Br J Pharmacol, 152, 959-979.

77. Lewis J., McGowan E., Rockwood J., Melrose H., Nacharaju P., Van Slegtenhorst M., Gwinn-Hardy K., Paul Murphy M., Baker M., Yu X., Duff K., Hardy J., Corral A., Lin W. L., Yen S. H., Dickson D. W., Davies P., and Hutton M. (2000) Neurofibrillary tangles, amyotrophy and progressive motor disturbance in mice expressing mutant (P301L) tau protein. Nat Genet, 4, 402-405.

78. Okawa Y., Ishiguro K., and Fujita S. C. (2003) Stress-induced hyperphosphorylation of tau in the mouse brain. FEBS Lett, 535, 183-189.

79. Yoshida S., Maeda M., Kaku S., Ikeya H., Yamada K., and Nakaike S. (2006) Lithium inhibits stress-induced changes in tau phosphorylation in the mouse hippocampus. J Neural Transm, 113, 1803–1814.

80. Sahara N., Vega I. E., Ishizawa T., Lewis J., McGowan E., Hutton M., Dickson D., and Yen S. H. (2004) Phosphorylated p38MAPK specific antibodies cross-react with sarkosyl-insoluble hyperphosphorylated tau proteins. J Neurochem, 90, 829-838.

81. Taniguchi S., Suzuki N., Masuda M., Hisanaga S., Iwatsubo T., Goedert M., and Hasegawa M. (2005) Inhibition of heparin-induced tau filament formation by phenothiazines, polyphenols, and porphyrins. J Biol Chem, 280, 7614-7623.

82. Ishihara T., Hong M., Zhang B., Nakagawa Y., Lee M. K., Trojanowski J. Q., and Lee V. M. (1999) Age-dependent emergence and progression of a tauopathy in transgenic mice overexpressing the shortest human tau isoform. Neuron, 3, 751-762.

83. Ishihara T., Zhang B., Higuchi M., Yoshiyama Y., Trojanowski J. Q., and Lee V. M. (2001) Age-dependent induction of congophilic neurofibrillary tau inclusions in tau transgenic mice. Am J Pathol, 158, 555-562.

84. Eckermann K., Mocanu M. M., Khlistunova I., Biernat J., Nissen A., Hofmann A., Schönig K., Bujard H., Haemisch A., Mandelkow E., Zhou L., Rune G., and Mandelkow E. M. (2007) The beta-propensity of Tau determines aggregation and synaptic loss in inducible mouse models of tauopathy. J Biol Chem, 282, 31755-31765.

85. Pérez M., Hernández F., Lim F., Díaz-Nido J., and Avila J. (2003) Chronic lithium treatment decreases mutant tau protein aggregation in a transgenic mouse model. J Alzheimers Dis, 5, 301-308.

86. Nakashima H., Ishihara T., Suguimoto P., Yokota O., Oshima E., Kugo A., Terada S., Hamamura T,. Trojanowski J. Q., Lee V. M., and Kuroda S. (2005) Chronic lithium

treatment decreases tau lesions by promoting ubiquitination in a mouse model of tauopathies. Acta Neuropathol, 110, 547-556.

87. Engel T., Goñi-Oliver P., Lucas J. J., Avila J., and Hernández F. (2006) Chronic lithium administration to FTDP-17 tau and GSK-3beta overexpressing mice prevents tau hyperphosphorylation and neurofibrillary tangle formation, but pre-formed neurofibrillary tangles do not revert. J Neurochem, 99, 1445-1455.
88. Martinez A. (2008) Preclinical efficacy on GSK-3 inhibitors: Towards a future generation of powerful drugs. Med Res Rev, 28, 773-796.
89. Augustinack J. C., Schneider A., Mandelkow E. M., and Hyman B. T. (2002) Specific tau phosphorylation sites correlate with severity of neuronal cytopathology in Alzheimer's disease. Acta Neuropathol, 103, 26-35.
90. Luna-Muñoz J, García-Sierra F., Falcón V., Menéndez I., Chávez-Macías L., and Mena R. (2005) Regional conformational change involving phosphorylation of tau protein at the Thr231, precedes the structural change detected by Alz-50 antibody in Alzheimer's disease. J Alzheimers Dis, 8, 29-41.
91. Steinhilb M. L., Dias-Santagata D., Mulkearns E. E., Shulman J. M., Biernat J., Mandelkow E. M., and Feany M. B. (2007) S/P and T/P phosphorylation is critical for tau neurotoxicity in Drosophila. J Neurosci Res, 85, 1271-1278.
92. Steinhilb M. L., Dias-Santagata D., Fulga T. A., Felch D. L., and Feany M. B. (2007) Tau phosphorylation sites work in concert to promote neurotoxicity in vivo. Mol Biol Cell, 18, 5060-5068.
93. Oka S., Shiraishi Y., Yoshida T., Ohkubo T., Sugiura Y., and Kobayashi Y. (2004) NMR structure of transcription factor Sp1 DNA binding domain. Biochemisty, 43, 16027-16035.

94. Ramanan V. K., Kim S., Holohan K., Shen L., Nho K., Risacher S. L., Foroud T. M., Mukherjee S., Crane P. K., Aisen P. S., Petersen R. C., Weiner M. W., Saykin A. J.; Alzheimer's Disease Neuroimaging Initiative (ADNI) (2012) Genome-wide pathway analysis of memory impairment in the Alzheimer's Disease Neuroimaging Initiative (ADNI) cohort implicates gene candidates, canonical pathways, and networks. Brain Imaging Behav, 6, 634-664.

95. Meng G., Zhong X., and Mei H. (2016) A systematic investigation into aging related genes in brain and their relationship with Alzheimer's disease. PloS One, 11, e0150624.

96. Subaiea G. M., Ahmed A. H., Adwan L. I., and Zawia N. H. (2015) Reduction of amyloid-β deposition and attenuation of memory deficits by tolfenamic acid. J Alzheimers Dis, 43, 425-433.

97. Adwan L., Subaiea G. M., Basha R., and Zawia N. H. (2015) Tolfenamic acid reduces tau and CDK5 levels: implications for dementia and tauopathies. J. Neurochem, 133, 266-272.

98. Wei C., Zhang W., Zhou Q., Zhao C., Du Y., Yan Q., Li Z., and Miao J. (2016) Mithramycin A alleviates cognitive deficits and reduces neuropathology in a transgenic mouse model of Alzheimer's disease. Neurochem Res, 41, 1924-1938.

99. Beishline K., and Azizkhan-Clifford J. (2015) Sp1 and the 'hallmarks of cancer'. FEBS J, 282, 224-258.

100. Cheng Q., Ling X., Haller A., Nakahara T., Yamanaka K., Kita A., Koutoku H., Takeuchi M., Brattain M. G., and Li F. (2012) Suppression of survivin promoter activity by YM155 involves disruption of Sp1-DNA interaction in the survivin core promoter. Int J Biochem Mol Biol, 3, 179-197.

101. Martin L., Latypova X., Wilson C. M., Magnaudeix A., Perrin M. L., Yardin C., and Terro F. (2013) Ageing Res Rev, 12, 289-309.

102. Meyerson M., Enders G. H., Wu C. L., Su L. K., Gorka C., Nelson C., Harlow E., and Tsai L. H. (1992) A family of human cdc2-related protein kinases. EMBO J, 1992, 11, 2909-2917.
103. Onishi T., Iwashita H., Uno Y., Kunitomo J., Saitoh M., Kimura E., Fujita H., Uchiyama N., Kori M., and Takizawa M. (2011) A novel glycogen synthase kinase-3 inhibitor 2-methyl-5-(3-{4-[(S)-methylsulfinyl]phenyl}-1-benzofuran-5-yl)-1,3,4-oxadiazole decreases tau phosphorylation and ameliorates cognitive deficits in a transgenic model of Alzheimer's disease. J Neurochem, 119, 1330-1340.
104. Patel P. and Woodgett J. R. (2017) Glycogen Synthase Kinase 3: A Kinase for All Pathways? Curr Top Dev Biol, 123, 277-302.
105. Shang S., Hua F., and Hu Z. W. (2017) The regulation of β-catenin activity and function in cancer: therapeutic opportunities. Oncotarget, 8, 33972-33989.
106. Giacobini E. and Gold G. (2013) Alzheimer disease therapy--moving from amyloid-β to tau. Nat Rev Neurol, 12, 677-686.
107. Medina M. and Avila J. (2014) New perspectives on the role of tau in Alzheimer's disease. Implications for therapy. Biochem Pharmacol, 88, 540-547.
108. Pedersen J. T. and Sigurdsson E. M. (2015) Tau immunotherapy for Alzheimer's disease. Trends Mol Med, 21, 394-402.
109. DeVos S. L., Miller R. L., Schoch K. M., Holmes B. B., Kebodeaux C. S., Wegener A. J., Chen G., Shen T., Tran H., Nichols B., Zanardi T. A., Kordasiewicz H. B., Swayze E. E., Bennett C. F., Diamond M. I., and Miller T. M. (2017) Tau reduction prevents neuronal loss and reverses pathological tau deposition and seeding in mice with tauopathy. Sci Transl Med, 9, eaag0481.